



**HAL**  
open science

## **Bidirectional drought-related canopy dynamics across pantropical forests: a satellite-based statistical analysis**

Liyang Liu, Fanxi Gong, Xiuzhi Chen, Yongxian Su, Lei Fan, Shengbiao Wu, Xueqin Yang, Jing Zhang, Wenping Yuan, Philippe Ciais, et al.

► **To cite this version:**

Liyang Liu, Fanxi Gong, Xiuzhi Chen, Yongxian Su, Lei Fan, et al.. Bidirectional drought-related canopy dynamics across pantropical forests: a satellite-based statistical analysis. *Remote Sensing in Ecology and Conservation*, 2022, 8 (1), pp.72-91. 10.1002/rse2.229 . hal-03604118

**HAL Id: hal-03604118**

**<https://hal.science/hal-03604118>**

Submitted on 11 Mar 2022

**HAL** is a multi-disciplinary open access archive for the deposit and dissemination of scientific research documents, whether they are published or not. The documents may come from teaching and research institutions in France or abroad, or from public or private research centers.

L'archive ouverte pluridisciplinaire **HAL**, est destinée au dépôt et à la diffusion de documents scientifiques de niveau recherche, publiés ou non, émanant des établissements d'enseignement et de recherche français ou étrangers, des laboratoires publics ou privés.



Distributed under a Creative Commons Attribution - NonCommercial - ShareAlike 4.0 International License

## ORIGINAL RESEARCH

# Bidirectional drought-related canopy dynamics across pantropical forests: a satellite-based statistical analysis

Liyang Liu<sup>1,2,3,4</sup> , Fanxi Gong<sup>1,2</sup>, Xiuzhi Chen<sup>1,2</sup>, Yongxian Su<sup>3</sup>, Lei Fan<sup>5</sup>, Shengbiao Wu<sup>6</sup>, Xueqin Yang<sup>1,3</sup>, Jing Zhang<sup>1,2</sup>, Wenping Yuan<sup>1,2</sup>, Philippe Ciais<sup>4</sup> & Chenghu Zhou<sup>3,7</sup>

<sup>1</sup>Guangdong Province Key Laboratory for Climate Change and Natural Disaster Studies, School of Atmospheric Sciences, Sun Yat-sen University, Zhuhai and 519082

<sup>2</sup>Southern Marine Science and Engineering Guangdong Laboratory (Zhuhai), Zhuhai 519082, China

<sup>3</sup>Key Laboratory of Guangdong for Utilization of Remote Sensing and Geographical Information System, Guangdong Open Laboratory of Geospatial Information Technology and Application, Guangzhou Institute of Geography, Guangzhou 510070, China

<sup>4</sup>Laboratoire des Sciences du Climat et de l'Environnement, IPSL, CEA-CNRS-UVSQ, Université Paris-Saclay, Gif sur Yvette 91191, France

<sup>5</sup>Chongqing Jinfo Mountain Karst Ecosystem National Observation and Research Station, School of Geographical Sciences, Southwest University, Chongqing 400715, China

<sup>6</sup>School of Biological Sciences, The University of Hong Kong, Pokfulam, Hong Kong

<sup>7</sup>State Key Laboratory of Resources and Environmental Information System, Institute of Geographical Sciences and Natural Resources Research, Chinese Academy of Sciences, Beijing 100101, China

## Keywords

Canopy variability, climate change, drought, satellite remote sensing, tropical forests, tropical phenology

## Correspondence

Xiuzhi Chen, Guangdong Province Key Laboratory for Climate Change and Natural Disaster Studies, School of Atmospheric Sciences, Sun Yat-sen University, Zhuhai 519082, China Tel: +86 0756-3668569; Fax: +86 0756-3668569; E-mail: chenxzh73@mail.sysu.edu.cn

Editor: Mat Disney

Associate Editor: Nicola Clerici

Received: 21 January 2021; Revised: 15 April 2021; Accepted: 14 June 2021

doi: 10.1002/rse2.229

[Correction added on 06 July 2021, after first online publication: city and postal code has been changed in affiliation 1 and correspondence section]

*Remote Sensing in Ecology and Conservation* 2022; **8** (1):72–91

## Introduction

Tropical forests are the largest terrestrial carbon dioxide sinks on Earth (Giardina et al., 2018) and play an essential role in the global carbon cycle (Asner et al., 2004). Even small changes in tropical forest dynamics could also

## Abstract

Droughts cause extreme anomalies in tropical forest growth, but the direction and magnitude of tropical forests in response to droughts are still widely debated. Here, we used four satellite-based canopy growth proxies (CGPs), including three optical and one passive microwave, and in situ fluxes observations from eddy covariance (EC) measurements for a retrospective investigation of the impacts of historical droughts on tropical forest growth from a statistical point of view. Results indicate two opposite directions in drought-related canopy dynamics across pantropical forests. The canopy of tropical forests with higher CGPs is more vulnerable to drought stress and recovers faster in the post-drought recovery period. In contrast, the canopy of tropical forests with lower CGPs increases during the drought period and declines in the subsequent recovery period, which is beyond general expectation. *In situ* measurements from eddy-covariance flux towers showed that forests with higher gross primary production and latent heat flux decreased photosynthesis and evapotranspiration during the drought period but increased photosynthesis and evapotranspiration faster during the post-drought recovery period, supporting the findings from satellite observations. Our statistical analysis against climatic factors predicts that higher-CGPs trees with probably taller and bigger canopies are more responsive to shortage of water availability caused by drought; while lower-CGPs trees with shorter and smaller canopies are more responsive to sunlight availability and tend to increase their canopy leaves and enhance photosynthesis in sunnier days during the drought period. Our results highlight the differences in tropical forests in responding to drought stress, which are worth incorporated in Earth system models for time-series evaluations.

affect the concentration of atmospheric CO<sub>2</sub> and thus global warming (Lewis et al., 2011; Phillips et al., 2009). In recent years, droughts have frequently occurred in tropical regions, depleting the soil water in tropical forests, inhibiting forest canopy photosynthesis, and even causing tree mortality (Baccini et al., 2017; Fan et al., 2019;

Wang et al., 2014). Tropical warming associated with global warming may further exacerbate the effects of droughts (Costa & Foley, 2000; Nepstad et al., 2004) on tropical forests and contribute to the reversal of the role of the tropical forests from being a carbon pool to a carbon source.

Tropical regions experienced several major droughts in 2005 (Chen et al., 2009; Marengo et al., 2008; Phillips et al., 2009; Saleska et al., 2007), 2010 (Lewis et al., 2011; Marengo et al., 2011) and 2015 (Jimenezmunoz et al., 2016; Panisset et al., 2018). Increasing sea surface temperature of the tropical Atlantic resulted in extensive Amazon droughts during the years 2005 and 2010 (Asefi-Najafabady & Saatchi, 2013; Marengo et al., 2011) and another strong El Niño-Southern Oscillation (ENSO) related drought event in 2015 (Doughty et al., 2015; Fan et al., 2019). Similarly, droughts were documented in 2005 (Asefi-Najafabady & Saatchi, 2013) and 2010 (Agha-Kouchak et al., 2015; Dutra et al., 2013; Lott et al., 2013) in Africa, and in 2015 in tropical Asia (Fan et al., 2019). In situ observations were conducted to investigate the impacts of tropical droughts on forest canopy growth and mortality (Anderegg et al., 2016; Gatti et al., 2014; Phillips et al., 2009). The results suggest that droughts may exceed the tolerance of tropical forests to water deficit, decreasing the stem biomass and increasing tree mortality (Asner & Alencar, 2010; Phillips et al., 2010; Wigneron et al., 2020). For example, the 2005 drought caused 1.2–1.6 Pg carbon loss of forest biomass, mostly via tree mortality (Asner & Alencar, 2010; Phillips et al., 2009). But this negative impact may not apply evenly to all types of forests across the pantropical region (Asner & Alencar, 2010). Studies found that droughts may kill tropical forests selectively (Phillips et al., 2009). Some studies show that fast-growing, softwood trees are more vulnerable to droughts (Hacke et al., 2001; McDowell et al., 2008). Some others showed that smaller trees, with diameters <40 cm at breast height, recover faster post-drought (Brando, 2018; da Costa et al., 2010; Fan et al., 2019; Rowland et al., 2015). However, site observations cannot directly measure the canopy growth status of plants at a large spatial scale (Konings & Gentine, 2017; Schimel et al., 2015), which makes it difficult to assess the large-scale ecological effects of droughts from field measurements alone (Asner & Alencar, 2010).

Remote sensing signals from spaceborne observations provide long-term time-series data with high-frequency for obtaining the spatial and temporal changes over forest properties in large regions (Zhang et al., 2016). The time-series data offer insights into the impacts of large-scale tropical droughts on forests, which are intensively observed but cannot be easily evaluated via field measurements alone (Asner & Alencar, 2010; Saatchi et al., 2013; Xu et al., 2011). The satellite-based canopy products are

one of the most widely used remotely sensed indicators to evaluate the impacts of forest droughts. Different from in situ experiments, which mainly focus on stem biomass, satellite-based canopy products reflect the canopy growth changes of tropical forests in reflectance caused by the loss of canopy leaves, canopy chlorophyll, or water content (Lee et al., 2013). For example, the upper-canopy characteristics (greenness, leaf area) of forests can directly reflect the canopy growth (Saatchi et al., 2013). The sensitivity of satellite spectral observations to the upper-canopy characteristics (greenness, leaf area) of forests thus is commonly used to estimate vegetation productivity (Saatchi et al., 2013; Zhao & Running, 2010).

Previous studies from satellite observations show great potential for satellite signals in representing the seasonality of canopy phenology and photosynthesis in tropical forests. Satellite optical remote sensing detected canopy green-up during the dry season in parts of Amazonian evergreen forests (Huete et al. 2006; Saleska et al., 2016; Xiao et al. 2005). However, the clouds, atmospheric aerosols and solar geometry might lead to contradictory results among different satellite observations (Malhi et al., 2009; Morton et al., 2014; Xu et al., 2011). For example, such a dry-season green-up pattern has been questioned (Jones et al., 2014; Morton et al., 2014; Samanta et al., 2011; Samanta et al., 2010) due to the near-infrared reflectance changes induced by cloud/aerosols contaminations and surface anisotropy. Recent analyses of optical data from multiple sensors showed that solar-induced fluorescence (SIF) could be used as an arguably better proxy of gross primary production (GPP) than optical data (Doughty et al., 2019; Lee et al., 2013; Xu et al., 2015), and that the enhanced vegetation index (Huete et al., 2006; Lopes et al., 2016; Wu et al., 2018) could also be considered as a proxy for leaf area change and new leaf flushing. Combining the above datasets, studies confirmed some regions of Amazonia being greener in the dry season period (Badgley et al., 2017; Guan et al., 2015) and identified distinct dry-minus-wet-season differences in canopy phenology between the northern wetter part of Amazonia where mean annual precipitation (MAP) >2000 mm year<sup>-1</sup> and other regions where MAP < 2000 mm year<sup>-1</sup> (Guan et al., 2015). Previous studies contributed great achievements in seasonal variations of phenology and photosynthesis. However, few substantial investigations were conducted on the response of the inter-annual variations of forest growth to large-scale drought events, which might differ from seasonal phenology (Asner & Alencar, 2010). For example, there are important differences between the dry season and drought in tropical forests, which are related to the geography, severity and persistence of precipitation deficit and cloud cover (Asner & Alencar, 2010). Studies suggested that severe drought

can exceed the dry-season tolerance of tropical forest canopies, resulting in decreased leaf area index (LAI) and a lowering of photosynthesis. In other words, although tropical forests are buffered to some degree from dry-season conditions (Nepstad et al., 1994), there are potential thresholds across which drought stress will cause losses in LAI and photosynthesis (Brando et al., 2008). Further research is needed to investigate the diverse interannual responses of tropical forests in responding to droughts, especially at a continental scale (Yang et al., 2018a, 2018b).

Differed from previous studies focus on dry-season 'green-up', this study mainly investigates the interannual responses of tropical forests to drought events. We hypothesize tropical forests have different tolerances to drought stresses and show diverse directions and magnitudes in interannual variations of canopy dynamics when encountering drought events. To comprehensively evaluate the impacts of droughts on tropical forest canopy growth, that is, canopy mass, water content and photosynthesis, we present the time series of four satellite-based canopy products to evaluate the drought loss and post-drought recovery during historical droughts in the tropical forests of Amazon, Africa and Asia from the 1980s to 2010s. In this paper, we selected four most widely used

remotely sensed indicators to evaluate the impacts of forest droughts, including three optical canopy products, that is, the LAI from Global Inventory Modeling and Mapping Studies (GIMMS LAI, Zhu et al., 2013), the near-infrared reflectance of terrestrial vegetation (NIRv) (Badgley et al., 2017) from moderate-resolution imaging spectroradiometer (MODIS) and reconstructed long-term continuous solar-induced chlorophyll fluorescence (CSIF) (Zhang et al., 2018a), and one passive microwave canopy product, that is, Ku-band vegetation optical depth (Ku-VOD, Moesinger et al., 2020). Here, we named such canopy parameters as the canopy growth proxies (CGPs). To define the drought events in tropical forests, we used the Palmer drought severity index (PDSI, Abatzoglou et al., 2018; Palmer, 1965; Zhao & Running, 2010) to evaluate the drought state of each pixel in the monthly PDSI and then to calculate the fractions of pixels in droughts across the tropical region to mark the drought years (red circles, Fig. 1) and recovery years (blue circles, Fig. 1) from 1985 to 2016 (Method). Besides, we also calculated the drought loss (denoted as  $\Delta\text{CGP}_{\text{drought}}$ ) and recovery gain (denoted as  $\Delta\text{CGP}_{\text{recovery}}$ ) of four CGPs during drought and recovery years (Method) to quantify tropical forests in response to droughts.

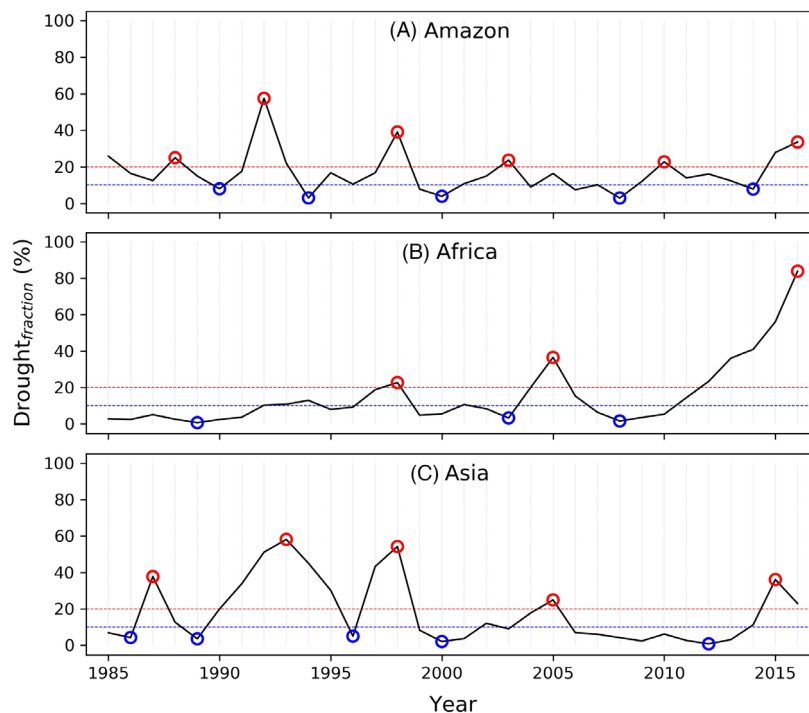


**Figure 1.** Long-term interannual dynamics of  $\text{Drought}_{\text{fraction}}$  of (A) Amazon (B) Africa and (C) Asia from 1980 to 2016. The troughs and peaks of  $\text{Drought}_{\text{fraction}}$  are categorized as drought years (red circles) and recovery years (blue circles), respectively. The red and blue dash lines represent  $\text{Drought}_{\text{fraction}}$  equals 20 and 10% respectively.

## Materials and Methods

### Study area

This study investigates the global tropical evergreen forests (TEF) based on the MODIS land cover map (MCD12C1, Sulla-Menashe & Friedl, 2018), Hansen forest cover map at the year 2000, and the annual deforestation maps from 2000 to 2016 (Hansen et al., 2013). First, we extracted all the pixels that belong to evergreen broadleaf forests (EBF) in the International Geosphere-Biosphere Programme (IGBP) classification in all tropical regions at 0.05° resolution from 2001 to 2016 and removed the pixels whose land types changed from 2001 to 2016. Then, we established a  $0.5 \times 0.5^\circ$  grid for the tropical areas and labeled EBF-dominated pixels, in which more than 50% of 0.05° pixels are tropical EBF. After that, for each 0.5° pixel, we further calculated the percentage of forest cover or affected by deforestation and removed pixel with a forest cover <70% or deforestation >20%.

The study area contains three regions: Amazon, Africa and tropical Asia (Fig. 2). Figure 2A Amazon (20°S–10°N by 50°W–80°W), comprising the largest and most biodiverse tract of tropical rainforest in the world. Figure 2B Africa (5°S–5°N by 10°E–30°E), the western part of the Africa TEF region, mainly in Cameroon, North Republic of Congo, Gabon and the Northwest Democratic Republic of the Congo. Figure 2C Tropical Asia (15°S–29°N by 92°E–150°E), covering the Indo-China Peninsula and the majority of the Malay Archipelago.

### Satellite-based canopy growth proxy (CGP) data

The CGP data include three optical datasets and one microwave satellite-based dataset. According to the satellite

signals, these four CGPs are divided into two categories: optical CGP (GIMMS LAI, MODIS NIRv and CSIF) and passive microwave CGP (Ku-band VOD) (Table S1).

### Optical CGPs

The GIMMS LAI dataset (Zhu et al., 2013) was derived from the advanced very high-resolution radiometer (AVHRR) measurements, computed using the GIMMS normalized difference vegetation index (NDVI), a neural network and the IGBP land cover classes (Zhu et al., 2013). Here, we adapted the newest version (4.0) GIMMS LAI which is available from 1985 to 2016 at a biweekly resolution and  $\sim 0.083^\circ$  spatial resolution (<http://cliveg.bu.edu/modismisr/lai3g-fpar3g.html>). And only pixels with the quality flag as 'good value' and 'Retrieved from spline interpolation' were used.

The NIRv was a new structural parameter of total scene near-infrared reflectance (NIR) and the NDVI (Badgley et al., 2017). The NIRv, which was strongly correlated with the fraction of photosynthetically active radiation, represented the proportion of pixel reflectance attributable to the vegetation in the pixel (Berry, 2018). Badgley et al. (2017) showed that MODIS NIRv is strongly correlated with GOME-2 SIF globally, as well as with site-level and grid-level GPP products.

The solar-induced chlorophyll fluorescence (SIF) has been previously reported to be capable of capturing the photosynthetic activity of terrestrial forests corresponding to drought (Lee et al., 2013; Liu et al., 2017). Such as GOME-2 SIF (Joiner et al., 2013, 2016), OCO-2 SIF (Frankenberg et al., 2014) and GOAST SIF (Lee et al., 2013). However, current satellite SIF datasets are limited for this study, due to the shorter available period, sensor degradation and spatial gap (Frankenberg et al., 2014; Zhang et al., 2018a, 2018b). Zhang et al. (2018a) used the

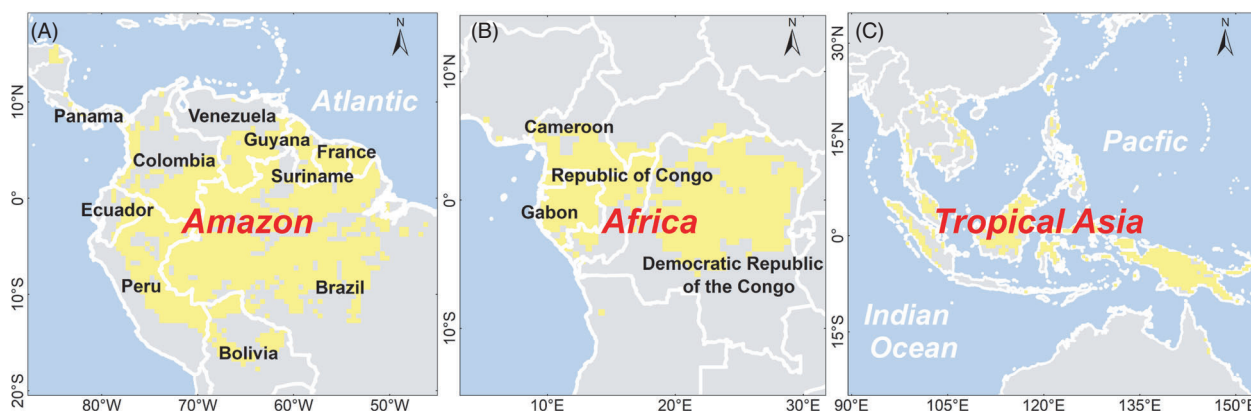


**Figure 2.** Study area. (A) Amazon (B) Africa and (C) Tropical Asia. The light-yellow pixels represent the evergreen broadleaf forests (EBF) pixels used in this study.

surface reflectance from MODIS and SIF from orbiting carbon observatory-2 (OCO-2) to generate long-term CSIF datasets based on machine learning algorithms. Here, we used all-sky daily SIF (CSIF<sub>all-day</sub>) from the CSIF dataset, which exhibits strong spatial, seasonal and inter-annual dynamics that are consistent with GOME-2 SIF and OCO-2 SIF (Zhang et al., 2018a).

### Passive Microwave CGP

The VOD is a passive microwave observation proportional to vegetation water content (Jackson & Schmugge, 1991; Van de Griend & Wigneron, 2004; Tian et al., 2018), which can be used to express the dynamic water content of canopy branches and leaves in tropical forests (Jones et al., 2013; Liu et al., 2015). Microwave VOD is sensitive to canopy variations at high biomass density, performing better than optical signals, which are usually saturated (Liu et al., 2018; Zhou et al., 2014). Here, we used a Ku-band VOD derived from VOD climate archive, which combines VOD observations from spaceborne sensors (SSM/I, TMI, AMSR-E, Windsat and AMSR-2) and removes their systematic differences (Moesinger et al., 2020). Compared with X-band (10.7 GHz, 1997–2018) and C-band (~6.9 GHz, 2002–2018) related products, the Ku-band VOD (~19 GHz, 1987–2017) has a longer time series, which is more useful for evaluating the impacts of historical droughts on tropical forests.

### Climate data

The downward shortwave solar radiation (SW<sub>down</sub>), air temperature (T<sub>air</sub>) and precipitation (PRE) data at the spatial resolution of 0.5° from 1985 to 2016 were obtained from the National Centers for Environmental Prediction (NCEP I and II) and Climatic Research Unit – NCEP (CRU-NCEP) version 7 (Viovy, 2018). The climate data were aggregated to the monthly temporal scale and resampled to 0.5° using the bilinear interpolation method (<http://rda.ucar.edu/datasets/ds314.3/>).

Atmospheric aridity and soil water deficit may limit plant carbon uptake and water use in terrestrial ecosystems (Novick et al., 2016). Here, we used the vapor pressure deficit (VPD) and Gravity Recovery and Climate Experiment (GRACE) terrestrial water storage (TWS) to represent the atmospheric aridity and soil water deficit, respectively. The VPD data were derived from the Integrated Forecast System of the European Centre for Medium-Range Weather Forecasts (ECMWF-IFS) (Yuan et al., 2019). We used the TWS datasets (GRACE-REC\_v03) by Humphrey and Gudmundsson (2019), which are based on two different GRACE solutions and three different meteorological forcing datasets (Humphrey & Gudmundsson, 2019).

### In situ data

The field observations with long time series were scarce across TEF. Here, we collected ground-based observations of three eddy covariance (EC) flux sites (Table S2) from the Fluxnet2015 dataset (Pastorello et al., 2020). As there is no in situ PDSI data along with the flux EC tower sites, we used the in situ precipitation as a surrogate to define the drought and recovery years (Wolf et al., 2016). Those years with annual precipitation lower than 5% of MAP were categorized as drought year and years which do not exceed this threshold were defined as recovery years. The field observed GPP and latent heat flux (LE) were used as proxies to represent the canopy growth status. We calculated the interannual dynamics in both GPP and LE between each drought year and each pre-/post-drought recovery year.

## Methods

### Detection of a drought pixel in a given month

Palmer drought severity index (Palmer, 1965) is a hydrological index based on the supply and demand concept of the water balance equation (Palmer, 1965). The PDSI has been widely used in detecting droughts across tropical forests (Wang et al., 2014; Zhao & Running, 2010). Here, the PDSI dataset was provided from 1985 to 2016 (Abatzoglou et al., 2018) and the detail can be found on the website (<http://www.climatologylab.org/terraclimate.html>). We used the time series monthly PDSI datasets from 1985 to 2016 (Abatzoglou et al., 2018) to calculate the monthly pixel-based standardized anomaly of the PDSI (PDSI<sub>anomaly</sub>).

$$\text{PDSI}_{\text{anomaly}} = (\text{PDSI}_{\text{month}} - \text{PDSI}_{\text{mean}}) / \text{PDSI}_{\text{stdev}}, \quad (1)$$

where PDSI<sub>month</sub> is the monthly PDSI, PDSI<sub>anomaly</sub> is the standardized anomaly of PDSI<sub>month</sub>, PDSI<sub>mean</sub> is mean value of the corresponding PDSI<sub>month</sub>, and PDSI<sub>stdev</sub> is the Standard Deviation (SD) of PDSI<sub>month</sub> from 1985 to 2016.

Then, we defined the pixel, whose PDSI<sub>anomaly</sub> is lower than  $-1$  SD, as a drought-impacted pixel on a monthly scale. We masked the pixels with PDSI<sub>anomaly</sub>  $> -1$  SD from the study area in the drought year. Similarly, we removed the pixels from the study area in each month of a recovery year, which were still impacted by drought using PDSI<sub>anomaly</sub>  $\leq -1$  SD. In that case, only those pixels, which encountered climatic drought stress in the drought year and became free from climatic drought stress in the recovery year, were considered in the analysis.

### Detection of drought and recovery years in three subregions

We calculated the annual percentage of drought pixels for Amazon, Africa and Asia (hereafter denoted as Drought<sub>fraction</sub>).

$$\text{Drought}_{\text{fraction}} = \frac{\sum_1^n \text{Count}_{\text{drought},i}}{\sum_1^n \text{Count}_{\text{total},i}}, \quad (2)$$

where  $n$  represents month from January to December,  $\text{Count}_{\text{drought},i}$  and  $\text{Count}_{\text{total},i}$  are the drought pixels and total pixels in a given month  $i$ , respectively. And  $\text{Count}_{\text{total},i}$  is a constant in each continent.

We compared the  $\text{Drought}_{\text{fraction}}$  peaks of long-term interannual variations with historical drought years (Table S3) and set an empirical  $\text{Drought}_{\text{fraction}}$  threshold of  $>20\%$  to define the drought year (red circles, Fig. 1). And this threshold can capture most of the drought year as literatures reported in Table S3. The troughs (blue circles, Fig. 1) of the  $\text{Drought}_{\text{fraction}}$  curve were categorized as recovery years, and we used an empirical threshold of lower than  $10\%$  to capture the relative wet recovery years.

### Statistics of CGP peaks and troughs

The selected four CGPs are from independent optical and passive microwave satellite sensors, which do not always show consistent interannual variations in either curve peaks or troughs, or in curve trends, that is, rising and falling directions. To derive a consistent time series of the four CGPs from 1985 to 2016, we first calculated the maximum monthly CGP at the pixel level in each year and then counted the regional yearly mean CGP in each continent, then we normalized the time-series regional CGPs variation.

$$\text{Normalized CGP} = \frac{\text{CGP} - \text{CGP}_{\text{min}}}{\text{CGP}_{\text{max}} - \text{CGP}_{\text{min}}}, \quad (3)$$

where CGP represents regional mean CGP in a given year,  $\text{CGP}_{\text{max}}$  and  $\text{CGP}_{\text{min}}$  represent the maximum and minimum time-series regional mean CGP, respectively.

By considering that different CGPs might be more related to different parameters, such as leaf area, water content, or photosynthesis, we assigned different weights ( $W$ ) to each CGP when the normalized CGP curve is at a peak ( $W = 1.0$ ) or a trough ( $W = 0.0$ ) or shows an increasing ( $W = 0.75$ ) or a decreasing trend ( $W = 0.25$ ). We finally calculated a new integrated CGP (denoted as  $\text{CGP}_{\text{integration}}$ ) from four satellite CGPs. Finally, the values of  $\text{CGP}_{\text{integration}}$  were stretched to 0–255 to obtain the gray background map in Figure 3.

$$\text{CGP}_{\text{integration}} = \sum_1^n W_i \times \text{CGP}_i, \quad (4)$$

where  $n$  represents the total CGPs number,  $n = 1-4$ ;  $W_i$  indicates the weight for  $\text{CGP}_i$ ;  $\text{CGP}_i$  represents the normalized CGPs.

### Evaluation of canopy growth loss ( $\Delta\text{CGP}_{\text{drought}}$ ) and recovered gain ( $\Delta\text{CGP}_{\text{recovery}}$ )

The datasets of four CGPs were aggregated at  $0.5^\circ$  spatial and monthly temporal resolutions based on the bilinear interpolation and average calculation methods, and the data gaps of each CGP data were filled by using linear interpolation. We first removed the effects of seasonal variations on the interannual variations of CGPs before, during and after droughts by subtracting the corresponding multiple-year monthly average value of each pixel. Then, we extracted the maximum monthly CGP values of each pixel based on the monthly CGPs from each pre-drought recovery year, drought year and post-drought recovery year to represent the interannual variations in CGPs before, during and after droughts, respectively. For each pixel, we calculated the CGP drought loss ( $\Delta\text{CGP}_{\text{drought}}$ ) by subtracting the CGP in the drought year from that in the former recovery year; and calculated the recovery gain ( $\Delta\text{CGP}_{\text{recovery}}$ ) by subtracting the CGP in the drought year from that in the subsequent recovery year. We then plotted  $\Delta\text{CGP}_{\text{drought}}$  against CGP in pre-drought recovery year and  $\Delta\text{CGP}_{\text{recovery}}$  against CGP in post-drought recovery year. All processes were conducted at pixel level for each drought event.

$$\Delta\text{CGP}_{\text{drought}} = \text{CGP}_{\text{drought}} - \text{CGP}_{\text{recovery}}^{\text{before}}, \quad (5)$$

$$\Delta\text{CGP}_{\text{recovery}} = \text{CGP}_{\text{recovery}}^{\text{after}} - \text{CGP}_{\text{drought}}, \quad (6)$$

where  $\text{CGP}_{\text{drought}}$  is the CGPs in the drought year;  $\text{CGP}_{\text{recovery}}^{\text{before}}$  and  $\text{CGP}_{\text{recovery}}^{\text{after}}$  are the CGPs in the recovery years before and after the given drought year, respectively. We only have one  $\Delta\text{CGP}_{\text{drought}}$  and  $\Delta\text{CGP}_{\text{recovery}}$  for each pixel for a specific drought or recovery year.

### Analyses of $\Delta\text{CGPs}$ with climatic interannual variability

In this study, we categorized climate factors into water-related factors (PRE, VPD and TWS) and radiation-related factors (SWdown and Tair). We analyzed the relationship between climate dynamics and CGP variations during the drought and recovery periods from water and radiation aspects. The calculation of interannual dynamics of climate parameters ( $\Delta\text{Climate}$ ) is the same as the calculation of  $\Delta\text{CGPs}$ .

## Results

### Performance of satellite-based CGPs in historical TEF droughts

We used the PDSI to calculate the regional percentage of the drought pixels ( $\text{Drought}_{\text{fraction}}$ ) (Fig. 1, Method).

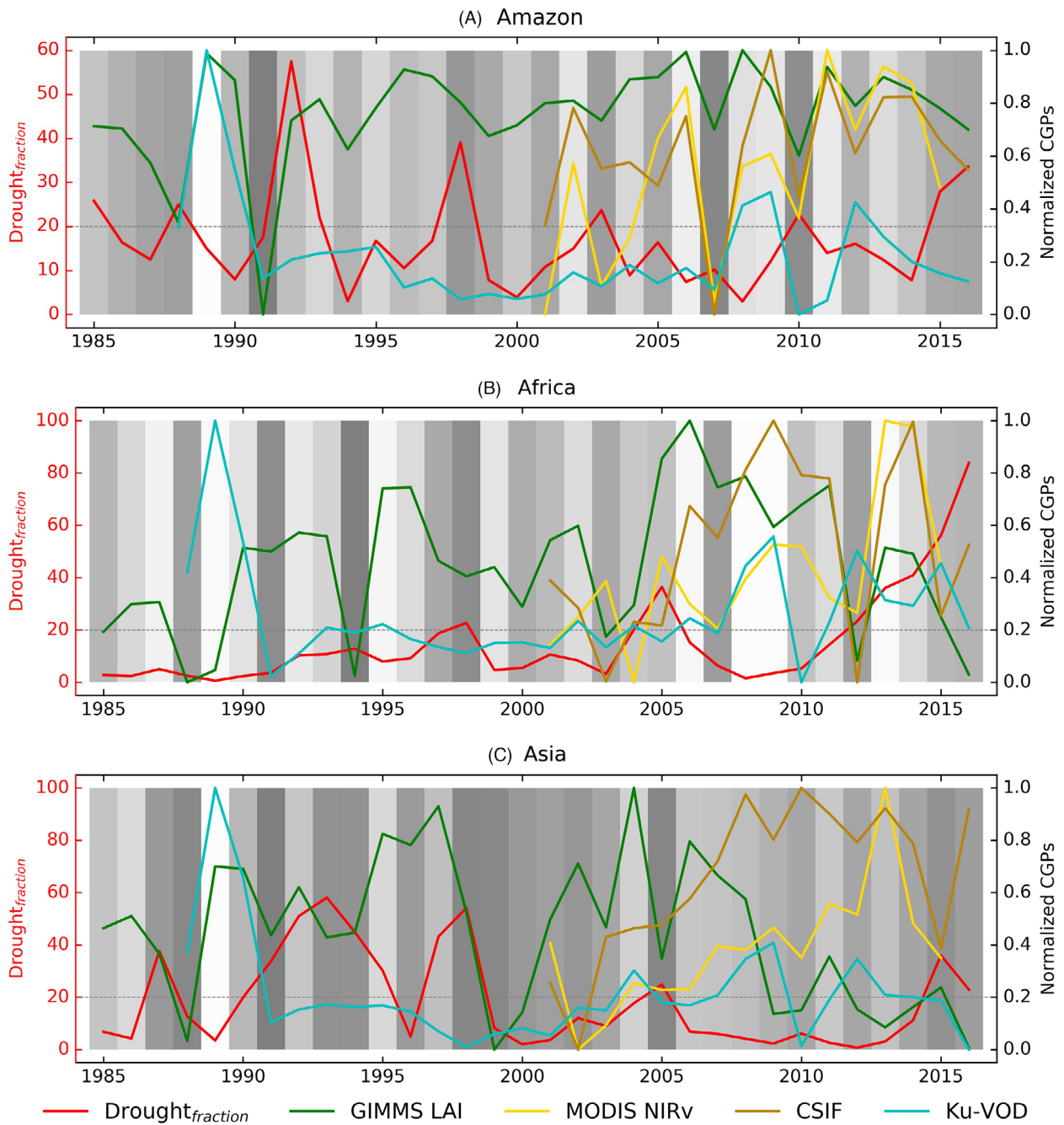


**Figure 3.** Historical climatic interannual dynamics represented by Drought<sub>fraction</sub> and interannual dynamics of canopy growth represented by four normalized CGPs of (A) Amazon (B) Africa and (C) Asia from 1985 to 2016. The gray background is integrated CGP (CGP<sub>integration</sub>) generated from four CGPs (Methods), which indicates the probability of tropical forests encountering the drought from low (light gray) to high (dark gray). CGPs, canopy growth proxies.

Figure 3 shows the Drought<sub>fraction</sub> curve (red curves in A, B, C) and the corresponding regional normalized CGP interannual dynamics over the past 30 years from 1985 to 2016. The time-series curve of Drought<sub>fraction</sub> was used to define the drought and recovery years, which represent

the corresponding historical climatic drought conditions in all tropical regions. The gray background color (CGP<sub>integration</sub>) in Figure 3 represents the probability of tropical forests encountering the drought illustrated by four CGPs (Method). The darker background indicates

the higher possibility as the drought years. The lighter background indicates the higher possibility as the recovery years.

The results (Fig. 3, Table S3) show that the years with the dark gray background, that is, the highest possibility of drought illustrated by four CGPs, coincide with the years with  $\text{Drought}_{\text{fraction}}$  peaks (red circles in Fig. 1) derived from the PDSI for most historical drought events: 1997/1998 (Espinoza et al., 2011; Nepstad et al., 2004), 2005 (Doughty et al., 2015), 2010 (Lewis et al., 2011) and 2015 (Doughty et al., 2015) in Amazonia (Figs. 1A and 3A), 2005 in Africa (Asefi-Najafabady & Saatchi, 2013) (Figs. 1B and 3B), and 1992/1993 (Sakai et al., 2006; Yoo et al., 2004), 1997/1998 (McVicar & Bierwirth, 2001) and 2015 (Fan et al., 2019) in tropical Asia (Figs. 1C and 3C). The proposed  $\text{CGP}_{\text{integration}}$  generally well agree with drought (darker background in Fig. 3) and recovery (lighter background in Fig. 3) years represented by  $\text{Drought}_{\text{fraction}}$  (Fig. 1), indicating that CGPs can detect the interannual dynamics of forest canopy before and after the short-term drought events, but the ranges of CGPs in different categories differ greatly, implying different impacts of droughts on different CGPs.

### Drought-related interannual dynamics of tropical canopy growth differ in directions and magnitudes

For each pixel per drought or recovery year, we plotted the drought loss (hereafter named  $\Delta\text{CGP}_{\text{drought}}$ ) and CGPs recovery gain (hereafter named  $\Delta\text{CGP}_{\text{recovery}}$ ) of four CGPs against their recovery CGPs, respectively (Fig. S1, Fig. 4). The results show that  $\Delta\text{GIMMS LAI}_{\text{drought}}$ ,  $\Delta\text{MODIS NIRv}_{\text{drought}}$ ,  $\Delta\text{Ku-VOD}_{\text{drought}}$  and  $\Delta\text{CSIF}_{\text{drought}}$  decrease from Low-CGP regions to High-CGP regions with a significant downward trend (Fig. 4, left). Conversely,  $\Delta\text{GIMMS LAI}_{\text{recovery}}$ ,  $\Delta\text{MODIS NIRv}_{\text{recovery}}$ ,  $\Delta\text{Ku-VOD}_{\text{recovery}}$  and  $\Delta\text{CSIF}_{\text{recovery}}$  of trees with higher CGPs increase dramatically compared to those with lower CGPs (Fig. 4, right). In other words, trees with higher values of GIMMS LAI (mean value  $>6.26 \pm 0.009$ , Mean  $\pm$  SEM, SEM is the standard error of the mean), MODIS NIRv (mean value  $>0.29 \pm 0.001$ ), CSIF (mean value  $>0.35 \pm 0.002$ ) and Ku-VOD (mean value  $>1.29 \pm 0.003$ ) are more vulnerable to drought stress (i.e., more negative  $\Delta\text{CGP}_{\text{drought}}$ ) and also show faster regrowth (i.e., more positive  $\Delta\text{CGP}_{\text{recovery}}$ ) than forests with lower-mean CGPs.

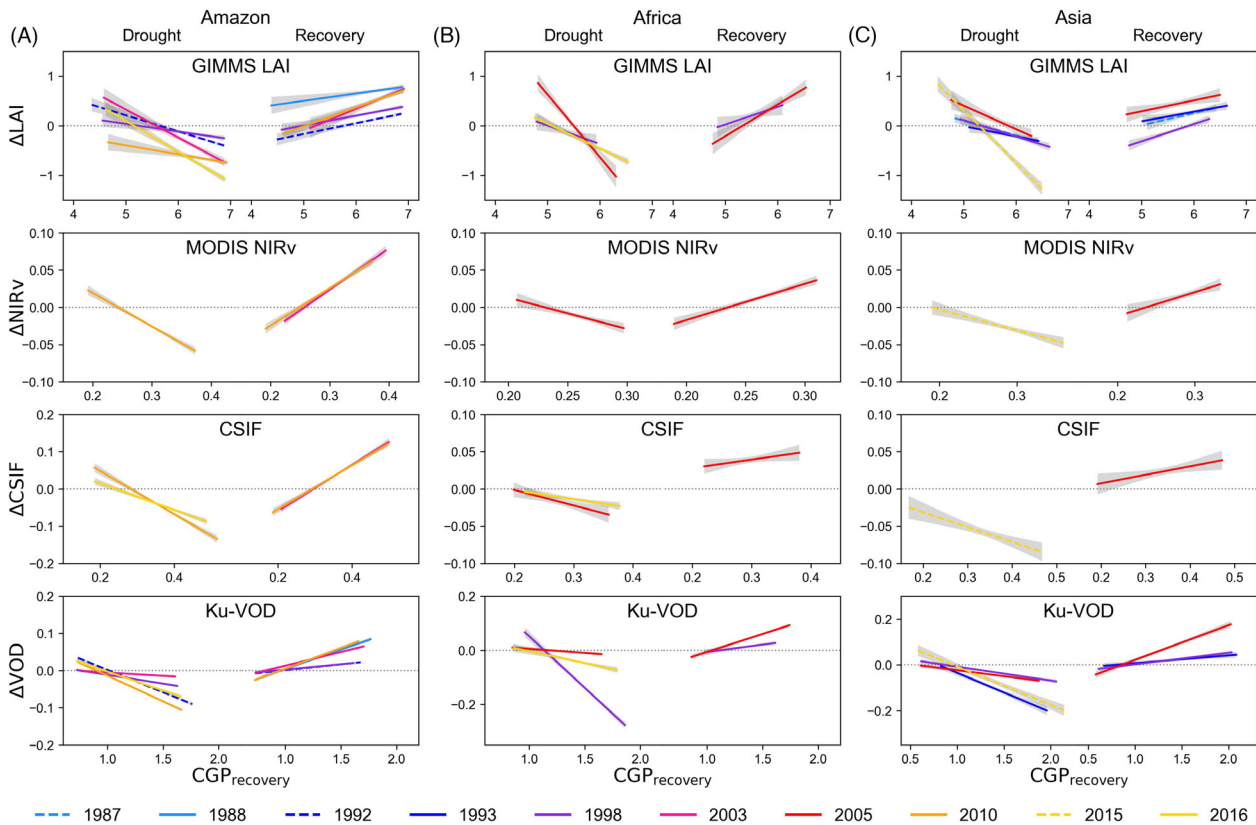


**Figure 4.** Interannual dynamics of forest growth proxies during drought period and post-drought period of (A) Amazon (B) Africa and (C) Asia. In each plot, the left curves are fitted curves of  $\Delta\text{CGP}_{\text{drought}}$  against CGP in pre-drought recovery year and the right curves are fitted curves of  $\Delta\text{CGP}_{\text{recovery}}$  against CGP in post-drought recovery year. The gray shadings represent the 95% confidence interval. CGP, canopy growth proxies.

Our results indicate another divergent direction in the interannual variability of tropical forests in drought response. Trees with lower GIMMS LAI (mean value  $<5.83 \pm 0.044$ ), MODIS-NIRv (mean value  $<0.27 \pm 0.001$ ), CSIF (mean value  $<0.33 \pm 0.003$ ) and Ku-VOD (mean value  $<1.13 \pm 0.017$ ) show positive values of  $\Delta\text{CGP}_{\text{drought}}$  during the drought period (Fig. 4). However, forests with sparse canopy leaves show significant 'green-up' during the drought period, which is opposite to decreasing greenness when well-grown forests face droughts. On the contrary, the canopy greenness of Low-CGP trees dims ( $\Delta\text{CGP}_{\text{recovery}} < 0$ ) after the drought events. The interannual dynamics of all four CGPs of tropical forests do not follow the general expectation, which mainly showed the negative impacts of droughts on tropical forests.

We further evaluated the impacts of droughts on interannual dynamics of forest growth, represented by the slopes of the linear fitted curves of CGPs in Figure 4. For the drought period, a steep slope indicates more positive  $\Delta\text{CGP}_{\text{drought}}$  in lower CGP pixels and more negative  $\Delta\text{CGP}_{\text{drought}}$  in higher CGP pixels (Fig. 5A) than a gentle slope. For the post-drought recovery period, a steep slope indicates more negative  $\Delta\text{CGP}_{\text{recovery}}$  in lower CGP pixels and more positive  $\Delta\text{CGP}_{\text{recovery}}$  in higher CGP pixels (Fig. 5B). Figure 6 shows that the slopes of the fitted curves of four CGPs (GIMMS LAI:  $R = 0.840$ ,  $P < 0.001$ ; MODIS NIRv:  $R = 0.965$ ,  $P < 0.001$ ; CSIF:  $R = 0.807$ ,  $P = 0.009$ ; Ku-VOD:  $R = 0.774$ ,  $P < 0.001$ ) (Table S4, Fig. 6) during the drought and post-drought period in Amazonia, Africa and tropical Asia are all positively related to  $\Delta\text{PDSI}$  (Fig. 6). Therefore, trees with higher mean CGPs show a more dramatic decrease in canopy growth, whereas trees with lower CGPs green up more significantly when they encounter a severe drought. The

divergent directions in interannual dynamics of drought-related forest canopy between sparse and well-grown canopies are amplified with the drought intensity.

To better understand the distribution of contradicting canopy behaviors in drought response, we averaged the drought-induced  $\Delta\text{CGP}_{\text{drought}}$  of each drought event and post-drought  $\Delta\text{CGP}_{\text{recovery}}$  of each recovery event for each CGP and overlapped them to locate the regions with  $\Delta\text{CGP}_{\text{drought}} < 0$  and  $\Delta\text{CGP}_{\text{recovery}} > 0$  (red pixels, Fig. 7) and regions with  $\Delta\text{CGP}_{\text{drought}} > 0$  and  $\Delta\text{CGP}_{\text{recovery}} < 0$  (blue pixels, Fig. 7). Results show that spatial patterns for all the four CGPs. Most tropical forests, as High-CGP type, decrease CGP during drought period and increase CGP after drought. The mean percentages are 77.90, 69.62 and 65.80% for Asia, Africa and America, respectively (Table S5). The tropical forests with  $\Delta\text{CGP}_{\text{drought}} > 0$  and  $\Delta\text{CGP}_{\text{recovery}} < 0$ , as Low-CGP type, are mainly located in the northwestern parts and central of Africa (e.g., Cameroon and the Democratic Republic of the Congo), Vietnam and central Papua New Guinea in tropical Asia. However, the spatial patterns of Low-CGP pixels are more complicated in Amazon illustrated by the four proxies, probably due to the complex forest biomes across Amazon (Sakschewski et al., 2016). This type of forests accounts for 8.67, 13.19 and 10.69% in Asia, Africa and America, respectively (Table S5).

### Forests in high-CGP and Low-CGP pixels exhibit varying interannual variabilities

To further explore the differences between high and low values of CGPs, based on the spatial pattern of Low-CGP and High-CGP of those four CGPs (Fig. 7), we further analyzed the interannual dynamics in canopy growth ( $\Delta\text{CGPs}$ ) with the corresponding interannual dynamics of

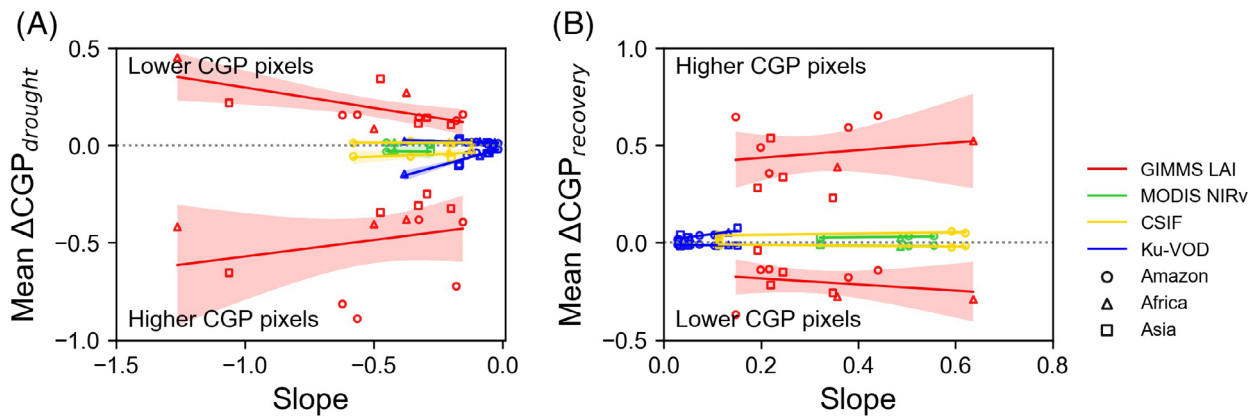


**Figure 5.** Scatter diagrams between the slopes of the linear fitting curves in Figure 4 and interannual dynamics of tropical forest CGPs during (A) drought loss ( $\Delta\text{CGP}_{\text{drought}}$ ) and (B) post-drought gain ( $\Delta\text{CGP}_{\text{recovery}}$ ) periods. The shadings represent the 95% confidence interval. CGPs, canopy growth proxies.

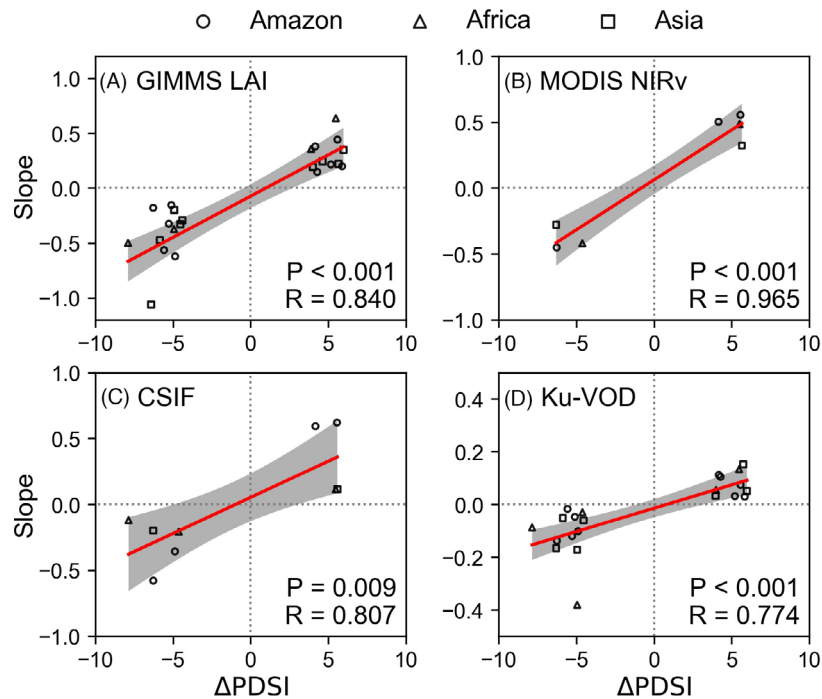


**Figure 6.** Interannual dynamics of tropical forest growth (A) GIMMS LAI (B) MODIS NIRv (C) CSIF and (D) Ku-VOD, represented by slopes of the linear fitting curves in Figure 4, with the interannual dynamics of climatic drought intensity represented by PDSI. The dots located at  $x < 0$  are the slopes of the fitting curves (left parts of each plot) during the drought period. The dots located at  $x > 0$  are the slopes of the fitting curves (right parts of each plot) during the post-drought period. The gray shadings represent the 95% confidence interval. PDSI, Palmer drought severity index.

climatic factors (i.e.,  $\Delta T_{air}$ ,  $\Delta SW_{down}$ ,  $\Delta VPD$ ,  $\Delta PRE$  and  $\Delta TWS$ ) during the drought or post-drought periods, respectively (Figs. S2–S5, Fig. 8).  $\Delta CGPs$  in High-CGP forests are positively related to  $\Delta PRE$  and  $\Delta TWS$  but negatively related to  $\Delta T_{air}$ ,  $\Delta SW_{down}$  and  $\Delta VPD$  (Figs. S2–S5, Fig. 8 red lines, Table S6). In contrast,  $\Delta CGPs$  in Low-CGP forests are negatively related to  $\Delta PRE$  and  $\Delta TWS$  but positively related to  $\Delta T_{air}$ ,  $\Delta SW_{down}$  and  $\Delta VPD$  (Figs. S2–S5, Fig. 8 blue lines, Table S7). This finding indicates that the High-CGP trees are more responsive to drought-related water deficits ( $\Delta VPD$ ,  $\Delta PRE$  and  $\Delta TWS$ ) (Table 1) and recover faster under sufficient water supply than Low-CGP trees. The Low-CGP forests, however, are more sensitive to light conditions ( $\Delta SW_{down}$ ) (Table 1), that is, tree canopy grows with higher  $T_{air}$  and  $SW_{down}$  but declines with more precipitation (more clouds and less light). This is probably because High-CGP trees, usually tall and old trees, show more water demand for transpiration and encounter longer transfer length due to greater canopy biomass and higher canopy height; whereas Low-CGP trees always with smaller biomass and shorter canopy height need less water supply for transpiration (Giardina et al., 2018; Phillips et al., 2010).

### Relationship between covariance measurements and satellite observations

The results of field observation showed that forests with higher GPP decreased photosynthesis during the drought period (Fig. 9A) but increased photosynthesis faster (Fig. 9B) during the post-drought recovery period. However, the forests with lower GPP showed opposite directions in responding to drought and post-drought recovery events. The LE analysis showed similar rules (Fig. 9C and D). We further analyzed the sensitivity of the interannual dynamics of GPP ( $\Delta GPP$ ) to the corresponding climate dynamics (i.e.,  $\Delta SW_{down}$ ,  $\Delta VPD$ ,  $\Delta PRE$ ) (Fig. S6). The results showed that the site with higher GPP (GF-Guy, mean  $GPP_{recovery} = 3755.70 \text{ gC m}^{-2} \text{ year}^{-1}$ ) is more positively sensitive to precipitation (slope = 0.006) than the site with lower GPP (MY-PSO, mean  $GPP_{recovery} = 2557.79 \text{ gC m}^{-2} \text{ year}^{-1}$ , slope = 0.001) and more negatively sensitive to VPD (slope:  $-7.121$  and  $-0.392$  for GF-Guy and MY-PSO, respectively) and  $SW_{down}$  (slope:  $-0.114$  and  $-0.025$  for GF-Guy and MY-PSO, respectively) (Table S8). In situ LE also showed similar results (Fig. S6D–F and Table S8). In situ observations support

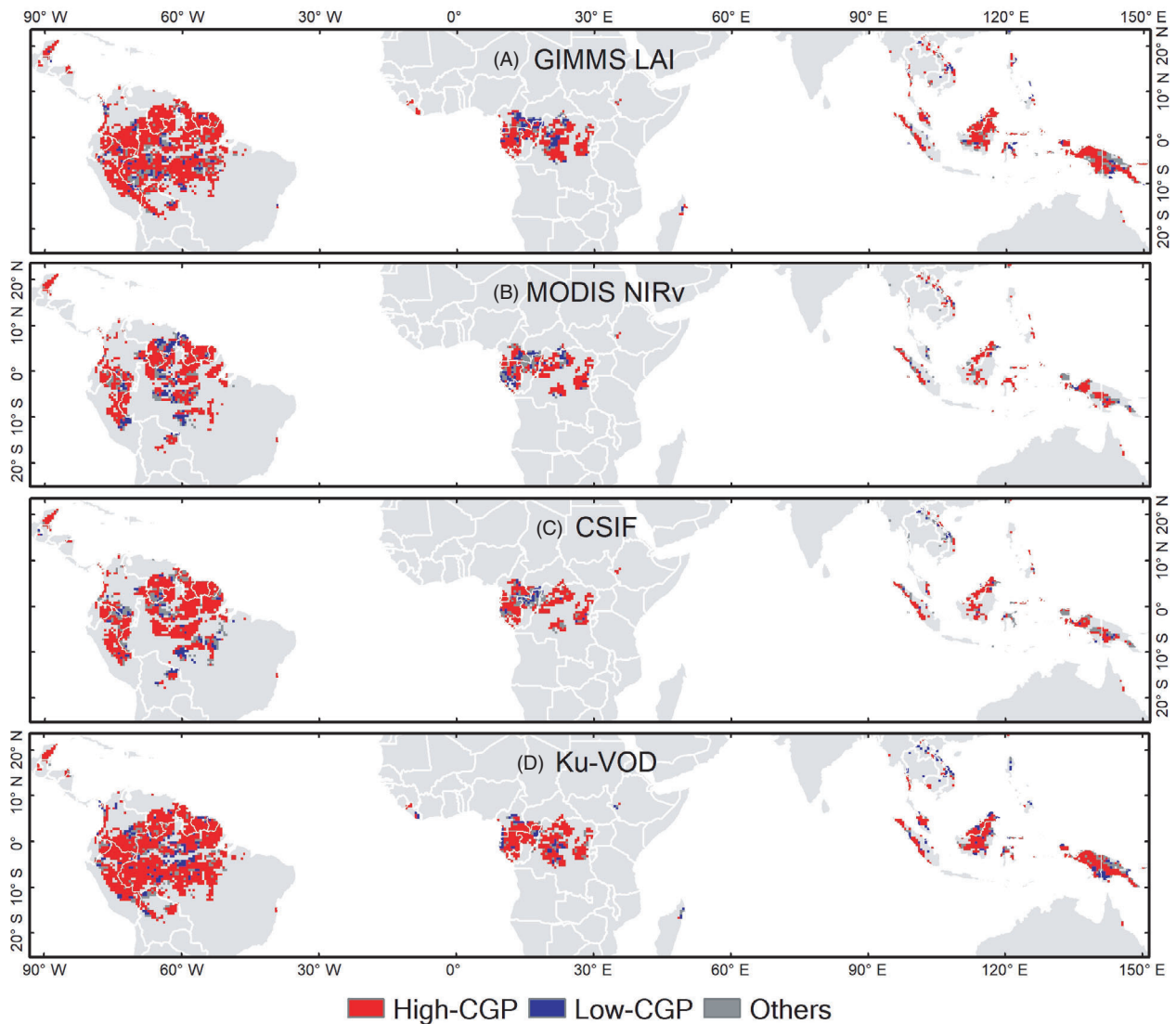


**Figure 7.** Spatial patterns of high-CGP (red pixels,  $\Delta\text{CGP}_{\text{drought}} < 0$  and  $\Delta\text{CGP}_{\text{recovery}} > 0$ ) and low-CGP (blue pixels,  $\Delta\text{CGP}_{\text{drought}} > 0$  and  $\Delta\text{CGP}_{\text{recovery}} < 0$ ) regions.  $\Delta\text{CGP}_{\text{drought}}$  and  $\Delta\text{CGP}_{\text{recovery}}$  are the mean values of several drought and recovery events from (A) 1985 to 2016, (B) 2001 to 2015, (C) 2000 to 2016 and (D) 1988 to 2016, respectively. The statistics of the percentage of high- and low-CGP of each continent are shown in Table S5. CGP, canopy growth proxies.

the findings from satellite observations that forests with High-CGPs are more vulnerable to drought stress due to water deficit and recovery faster because of sufficient water supply (Figs. 4 and 8).

## Discussion

### Evaluations of potential uncertainty between the drought indicators

The drought event itself and its impacts on tropical forests are complex, which are still poorly understood

(AghaKouchak et al., 2015; Asner & Alencar, 2010; Van Emmerik et al., 2017). PDSI can well characterize the global surface water conditions and water flow conditions (Dai et al., 2004) and thus can comprehensively assess drought conditions caused by water and heat stress, and is more commonly used in tropical studies (Lima & AghaKouchak, 2017; Raphael et al., 2017). To explore potential uncertainty introduced by different choices of drought indicators, besides the PDSI, we added another widely used drought index in long-term large-scale research—the standardized precipitation index (SPI) (McKee et al., 1993), which is available until 2012 and

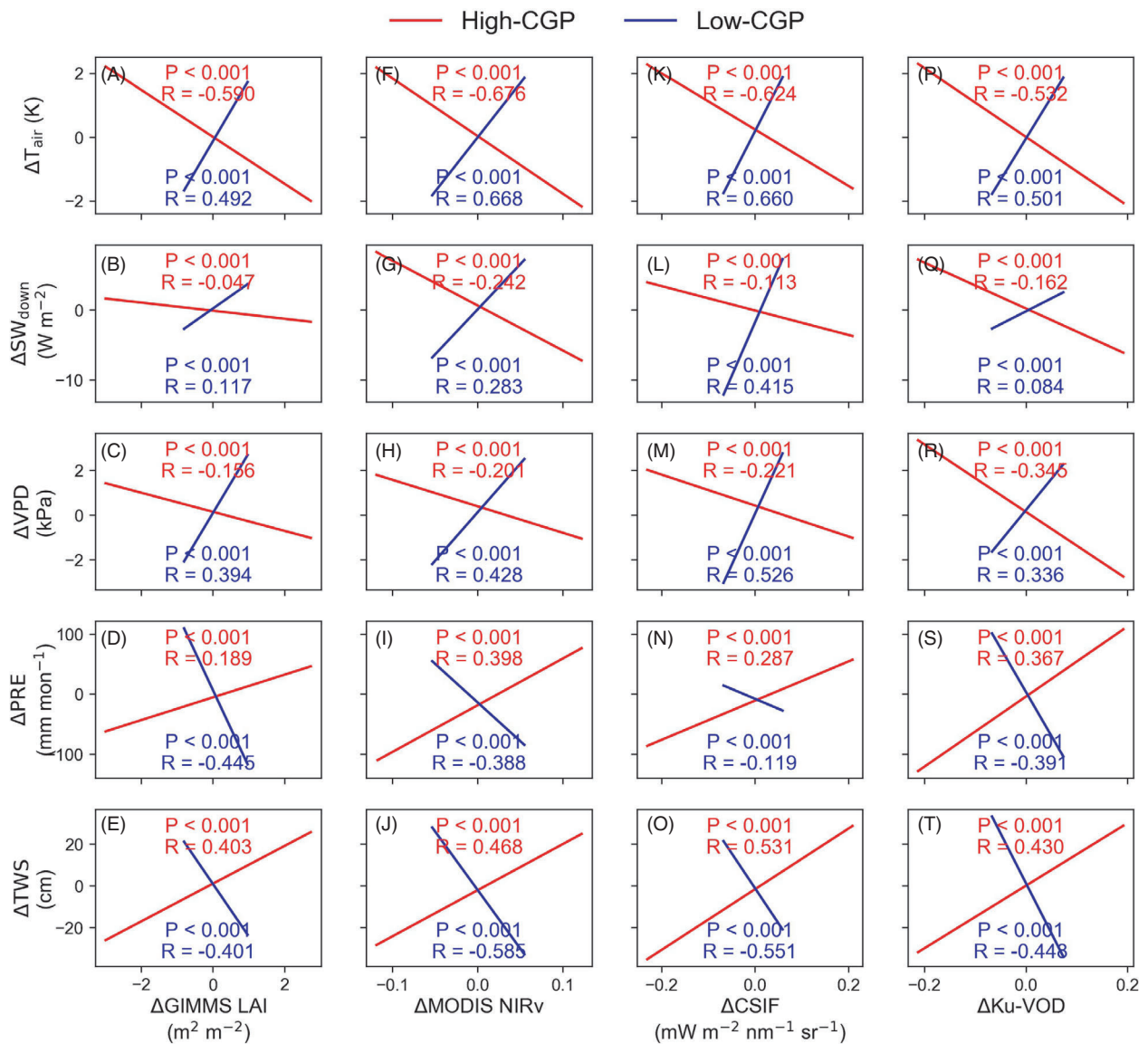


**Figure 8.** Scatter diagrams of interannual dynamics of canopy growth ( $\Delta$ CGPs) versus corresponding climatic interannual dynamics (i.e.,  $\Delta T_{air}$ ,  $\Delta SW_{down}$ ,  $\Delta VPD$ ,  $\Delta PRE$  and  $\Delta TWS$ ). (A-E) GIMMS LAI, (F-J) MODIS NIRv, (K-O) CSIF, (P-T) Ku-VOD. The Y axes from the first row to the last row are  $\Delta T_{air}$ ,  $\Delta SW_{down}$ ,  $\Delta VPD$ ,  $\Delta PRE$  and  $\Delta TWS$ , respectively. The red lines represent high-CGPs and the blue lines represent low-CGPs.

**Table 1.** Opposite directions in canopy dynamics between high-CGP and low-CGP trees.

	High-CGP trees	Low-CGP trees
Drought period	Negative $\Delta CGP_{drought}$	Positive $\Delta CGP_{drought}$
Recovery period	Positive $\Delta CGP_{recovery}$	Negative $\Delta CGP_{recovery}$
Climate sensitivity	More sensitive to water availability	More sensitive to sunlight availability

CGP, canopy growth proxies.

provided with 3-, 6-, and 12-month scales, downloaded from the National Center for Atmospheric Research/University Corporation for Atmospheric Research (2013). We calculated drought fractions for each continent and each year ( $Drought_{fraction, SPI}$ ) based on the same method as PDSI (Equation 2). The results (Fig. S7) showed that the  $Drought_{fraction, SPI}$  mostly captured drought years as categorized by PDSI (Fig. S8).

It is worth noting that, since the 2000s, there were three reported severe drought events (2005, 2010 and 2015) (Table S3) in the Amazon. The proposed  $Drought_{fraction}$

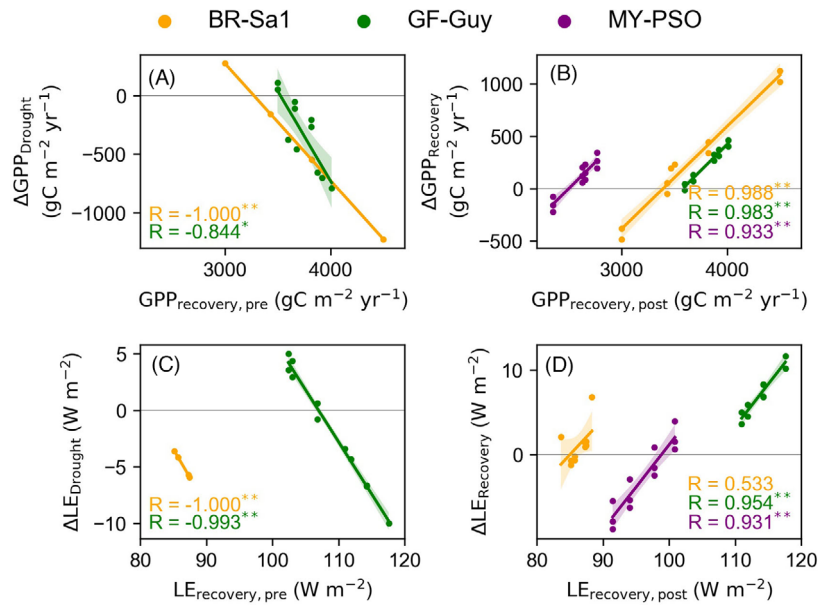


**Figure 9.** Interannual dynamics of in situ GPP and LE during the drought period (A and C) and post-drought period (B and D). The  $GPP_{recovery,pre}$  and  $GPP_{recovery,post}$  in X axis are the GPP values of pre- and post-drought recovery years, respectively;  $LE_{recovery,pre}$  and  $LE_{recovery,post}$  in X axis are the LE values of pre- and post-drought recovery years, respectively. The shadings represent the 95% confidence interval. The \* indicate  $P < 0.05$  and \*\* represent  $P \leq 0.001$ . GPP, gross primary production; LE, latent heat flux.

captured the droughts in 2010 and 2015 but failed in representing severe drought in occurred in the southwestern Amazon from July to September in 2005 (Yang et al., 2018a, 2018b) (Fig. S9). That is because in this study, we considered the whole tropical EBF pixels and used the  $Drought_{fraction}$  to define the drought year. However, there was only a small  $Drought_{fraction}$  at monthly scale during August to October in 2005 (Fig. S10), which can be seen as in comparison with the 2003 drought. The  $Drought_{fraction}$  in 2005 (16.3%) has a small peak (Fig. 1A), being lower than the 20% threshold and thus the year 2005 was not categorized as a drought year in this study.

### The CGPs represent different physiological features of tropical trees in response to droughts

Using the satellite-based optical CGPs (LAI, NIRv and CSIF) and passive microwave CGP (Ku-VOD), we comprehensively assessed the impacts of droughts on the forest canopy. However, different CGPs might be related to different features, such as leaf area, water content, or photosynthesis. The LAI, as one of the most basic parameters to describe the vegetation canopy structure, is related to canopy mass cover. The NIRv provides information on the fractional absorption of sunlight and photosynthetic capacity (Zhao & Running, 2010). The SIF, as an early indicator of physiological alterations for global monitoring

of vegetation (Hernández-Clemente et al., 2017), is very sensitive to the response of vegetation environmental stress and has certain technical advantages in detecting early vegetation stress (Liu et al., 2013). When a tree experiences drought stress, it will first increase heat dissipation with a subsequent decrease in both photochemistry and fluorescence (Daumard et al., 2010; Flexas et al., 2002; Galmés et al., 2007). As the drought continues, the tree will reduce water stress through increase falling of leaves, or even cause tree mortality (Baccini et al., 2017; Fan et al., 2019; Wang et al., 2014), and both these two behaviors will decrease LAI. Although optical indices are vulnerable to the effects of clouds, atmospheric action, aerosols, water vapor and land cover (AghaKouchak et al., 2015; Andela et al., 2013; Shi et al., 2008), consistent results were detected in both canopy mass-related CGP (LAI) and photosynthesis-related CGPs (NIRv and SIF).

With less saturation and higher penetration than optical signals, the microwave VOD is a more robust proxy to represent the variations in vegetation water content of tropical forests (Chen et al., 2020; Fan et al., 2019). Our result showed that Ku-VOD has the same response to drought as optical signals and Ku-VOD can capture the more depth variations of canopy than optical ones, although the Ku band has a lower penetration depth when compared with lower frequency VOD such as L-VOD, which contains less information on deeper vegetation layers. The Ku-VOD, as a potential canopy

water/mass-related proxy, provides a unique signal for capturing tropical forest canopy changes in response to droughts (AghaKouchak et al., 2015).

### **The sensitivity to climate interannual variability controls the directions and magnitudes of drought-related CGPs interannual variations**

We found that forests of High-CGP and Low-CGP pixels show opposite directions and diverse magnitudes in response to climate interannual variability (Fig. 8, Table 1). High-CGP trees show large declines in canopy growth during droughts and fast recovery post-drought, whereas Low-CGP trees show an increase in canopy growth under drought conditions but a decrease in the recovery period. Generally, High-CGP trees are usually taller and bigger ones; while Low-CGP trees are relatively smaller ones. Taller and bigger trees have proportionally more leaves supported by the same area of xylem than smaller trees (Liu et al., 2019; McDowell et al., 2002). The reduction in the total water consumption of taller and bigger trees is more severe under drought than that of smaller trees. This is consistent with our satellite-based findings that the High-CGP forests are more sensitive to water availability, and thus are more responsive to water stress during drought periods. Some site experiments observed higher mortality of trees with large and dense canopies (Anderegg et al., 2016; Brando, 2018; Phillips et al., 2010), supporting our hypothesis that the shortage of water availability caused by drought has a huge negative impact on High-CGP trees. In contrast, Low-CGP forests are likely smaller and shorter ones with sparse canopies, which are more sensitive to sunlight availability. Therefore, Low-CGP trees tend to absorb more radiation and increase their canopy leaves and enhance photosynthesis on sunnier days during the drought period.

It is also worth noting that VPD is a comprehensive climatic parameter related to both air temperature and atmospheric humidity (Aumann & Pagano, 1994). Air temperature and atmospheric humidity can boost photosynthesis in high VPD conditions due to the increase in  $T_{air}$  (Yuan et al., 2019) but can also depress photosynthesis under severe VPD conditions due to water deficit (Lee & Boyce, 2010; Reichstein et al., 2002). Chen et al. (2020, 2021) have demonstrated that VPD can be considered as a trigger of the dry-season canopy 'green-up' across Amazonian evergreen forests. Our findings also indicate the great potential of VPD as a trigger of canopy growth dynamics responding to short-term droughts, which is important for modeling the carbon-water cycle in terrestrial tropical ecosystems.

## **Conclusions and Recommendations**

Both satellite-observed signals and in situ observed fluxes were used to examine two types of forests (i.e., both higher and lower CGPs trees) with divergent directions and magnitudes in interannual variability of canopy growth during drought and recovery periods. The analysis shows that the two directions of forest canopy changes are mainly related to different underlying mechanisms in responding to sunlight and water variations. The results highlight the differences of tropical forests in responding to drought stress, which is worth incorporated in land surface models (LSMs). By neglecting to account for the differences of forest canopy covers, LSMs tend to underestimate the impacts of drought on dense canopy-cover forests but overestimate those impacts on sparse canopy-cover forests. Our findings are critical for assessing global carbon and water cycles, which are poorly considered in global land surface models. Understanding the characteristics of CGPs and the forest itself is extremely essential for maintaining the carbon-water balance and is critical for assessing global carbon and water cycles.

This study detected opposite canopy behaviors across pantropical forests in response to drought events; while we did not take into account the impacts of drought intensity and drought duration. In addition, further investigations are needed to explore mechanisms of opposite drought-related canopy behaviors of tropical forests in the future.

## **Acknowledgments**

This research was funded by the National Key Research and Development Program of China, grant number 2016YFA0602701; the National Natural Science Foundation of China, grant numbers 31971458 and 41971275; Innovation Group Project of Southern Marine Science and Engineering Guangdong Laboratory (Zhuhai), grant number 311021009; the Guangdong Basic and Applied Basic Research Foundation, grant number 2020A151501091; GDAS Special Project of Science and Technology Development, grant number 2020GDASYL-20200102002.

## **Conflict of Interest**

The authors declare that there is no conflict of interest.

## **Funding Information**

This research was funded by the National Key Research and Development Program of China, grant number 2016YFA0602701; National Natural Science Foundation

of China, grant numbers 31971458 and 41971275; Innovation Group Project of Southern Marine Science and Engineering Guangdong Laboratory (Zhuhai), grant number 311021009; the Guangdong Basic and Applied Basic Research Foundation, grant number 2020A151501091; GDAS Special Project of Science and Technology Development, grant number 2020GDASYL-20200102002.

## References

- Abatzoglou, J.T., Dobrowski, S.Z., Parks, S.A. & Hegewisch, K.C. (2018) TerraClimate, a high-resolution global dataset of monthly climate and climatic water balance from 1958–2015. *Scientific Data*, **5**, 170191. <https://doi.org/10.1038/sdata.2017.191>
- Aghakouchak, A., Farahmand, A., Melton, F., Teixeira, J.P., Anderson, M.C., Wardlow, B.D. et al. (2015) Remote sensing of drought: progress, challenges and opportunities. *Reviews of Geophysics*, **53**(2), 452–480. <https://doi.org/10.1002/2014RG000456>
- Andela, N., Liu, Y.Y., van Dijk, A.I.J.M., de Jeu, R.A.M. & McVicar, T.R. (2013) Global changes in dryland vegetation dynamics (1988–2008) assessed by satellite remote sensing: comparing a new passive microwave vegetation density record with reflective greenness data. *Biogeosciences Discussions*, **10**, 8749–8797. <https://doi.org/10.5194/bg-10-6657-2013>
- Anderegg, W.R.L., Klein, T., Bartlett, M., Sack, L., Pellegrini, A.F.A., Choat, B. et al. (2016) Meta-analysis reveals that hydraulic traits explain cross-species patterns of drought-induced tree mortality across the globe. *Proceedings of the National Academy of Sciences of the United States of America*, **113**, 5024–5029. <https://doi.org/10.1073/pnas.1525678113>
- Asefi-Najafabady, S. & Saatchi, S. (2013) Response of African humid tropical forests to recent rainfall anomalies. *Philosophical Transactions of the Royal Society B: Biological Sciences*, **368**(1625), 20120306. <https://doi.org/10.1098/rstb.2012.0306>
- Asner, G.P. & Alencar, A. (2010) Drought impacts on the Amazon forest: the remote sensing perspective. *New Phytologist*, **187**(3), 569–578. <https://doi.org/10.1111/j.1469-8137.2010.03310.x>
- Asner, G.P., Nepstad, D.C., Cardinot, G. & Ray, D. (2004) Drought stress and carbon uptake in an Amazon forest measured with spaceborne imaging spectroscopy. *Proceedings of the National Academy of Sciences of the United States of America*, **101**(16), 6039–6044. <https://doi.org/10.1073/pnas.0400168101>
- Aumann, H.H. & Pagano, R.J. (1994) Atmospheric infrared sounder on the earth observing system. *Optical Engineering*, **33**(3), 776–785. <https://doi.org/10.1073/pnas.0400168101>
- Baccini, A., Walker, W., Carvalho, L., Farina, M., Sulla-Menashe, D. & Houghton, R.A. (2017) Tropical forests are a net carbon source based on aboveground measurements of gain and loss. *Science*, **358**(6360), 230–234. <https://doi.org/10.1126/science.aam5962>
- Badgley, G., Field, C.B. & Berry, J.A. (2017) Canopy near-infrared reflectance and terrestrial photosynthesis. *Science Advances*, **3**(3), e1602244. <https://doi.org/10.1126/sciadv.1602244>
- Berry, J. (2018). 3.10 solar induced chlorophyll fluorescence: origins, relation to photosynthesis and retrieval.
- Brando, P. (2018) Tree height matters. *Nature Geoscience*, **11**, 390–391. <https://doi.org/10.1038/s41561-018-0147-z>
- Brando, P.M., Nepstad, D.C., Davidson, E.A., Trumbore, S.E., Ray, D. & Camargo, P. (2008) Drought effects on litterfall, wood production and belowground carbon cycling in an Amazon forest: results of a throughfall reduction experiment. *Philosophical Transactions of the Royal Society B: Biological Sciences*, **363**(1498), 1839–1848. <https://doi.org/10.1098/rstb.2007.0031>
- Chen, J., Wilson, C.R., Tapley, B.D., Yang, Z. & Niu, G. (2009) 2005 drought event in the Amazon River basin as measured by GRACE and estimated by climate models. *Journal of Geophysical Research*, **114**, B05404. <https://doi.org/10.1029/2008JB006056>
- Chen, X., Maignan, F., Viovy, N., Bastos, A., Goll, D., Wu, J. et al. (2020) Novel representation of leaf phenology improves simulation of amazonian evergreen forest photosynthesis in a land surface model. *Journal of Advances in Modeling Earth Systems*, **12**, e2018MS001565. <https://doi.org/10.1029/2018MS001565>
- Chen, X., Ciais, P., Maignan, F., Zhang, Y., Bastos, A., Liu, L. et al. (2021) Vapor pressure deficit and sunlight explain seasonality of leaf phenology and photosynthesis across Amazonian evergreen broadleaved forest. *Global Biogeochemical Cycles*, **35**(6), e2020GB006893. <https://doi.org/10.1029/2020gb006893>
- Costa, M.H. & Foley, J.A. (2000) Combined effects of deforestation and doubled atmospheric CO<sub>2</sub> concentrations on the climate of Amazonia. *Journal of Climate*, **13**(1), 18–34. [https://doi.org/10.1175/1520-0442\(2000\)013<0018:CEODAD>2.0.CO;2](https://doi.org/10.1175/1520-0442(2000)013<0018:CEODAD>2.0.CO;2)
- da Costa, A.C.L., Galbraith, D., Almeida, S., Portela, B.T.T., da Costa, M., Junior, J.A.S. et al. (2010) Effect of 7 yr of experimental drought on vegetation dynamics and biomass storage of an eastern Amazonian rainforest. *New Phytologist*, **187**(3), 579–591. <https://doi.org/10.1111/j.1469-8137.2010.03309.x>
- Dai, A., Trenberth, K.E. & Qian, T. (2004) A global dataset of palmer drought severity index for 1870–2002: relationship with soil moisture and effects of surface warming. *Journal of Hydrometeorology*, **5**, 1117–1130. <https://doi.org/10.1175/JHM-386.1>
- Daumard, F., Champagne, S., Fournier, A., Goulas, Y., Ounis, A., Hanocq, J.-F. et al. (2010) A field platform for continuous measurement of canopy fluorescence. *IEEE Transactions on Geoscience and Remote Sensing*, **48**(9), 3358–3368. <https://doi.org/10.1109/TGRS.2010.2046420>

- Doughty, C.E., Metcalfe, D.B., Girardin, C.A.J., Amézquita, F.F., Cabrera, D.G., Huasco, W.H. et al. (2015) Drought impact on forest carbon dynamics and fluxes in Amazonia. *Nature*, **519**(7541), 78. <https://doi.org/10.1038/nature14213>
- Doughty, R., Köhler, P., Frankenberg, C., Magney, T.S., Xiao, X., Qin, Y. et al. (2019) TROPOMI reveals dry-season increase of solar-induced chlorophyll fluorescence in the Amazon forest. *Proceedings of the National Academy of Sciences of the United States of America*, **116**(44), 22393–22398. <https://doi.org/10.1073/pnas.1908157116>
- Dutra, E., Magnusson, L., Wetterhall, F., Cloke, H.L., Balsamo, G., Boussetta, S. et al. (2013) The 2010–2011 drought in the Horn of Africa in ECMWF reanalysis and seasonal forecast products. *International Journal of Climatology*, **33**(7), 1720–1729. <https://doi.org/10.1002/joc.3545>.
- Espinoza, J.C., Ronchail, J., Guyot, J.L., Junquas, C., Vauchel, P., Lavado, W. et al. (2011) Climate variability and extreme drought in the upper Solimões River (western Amazon Basin): understanding the exceptional 2010 drought. *Geophysical Research Letters*, **38**(13), n/a–n/a. <https://doi.org/10.1029/2011GL047862>
- Fan, L., Wigneron, J.P., Ciais, P., Chave, J., Brandt, M., Fensholt, R. et al. (2019) Satellite-observed pantropical carbon dynamics. *Nature Plants*, **5**(9), 944–951. <https://doi.org/10.1038/s41477-019-0478-9>
- Flexas, J., Escalona, J.M., Evain, S., Gulías, J., Moya, I., Osmond, C.B. et al. (2002) Steady-state chlorophyll fluorescence (Fs) measurements as a tool to follow variations of net CO<sub>2</sub> assimilation and stomatal conductance during water-stress in C3 plants. *Physiologia Plantarum*, **114**, 231–240. <https://doi.org/10.1034/j.1399-3054.2002.1140209.x>
- Frankenberg, C., O'Dell, C., Berry, J., Guanter, L., Joiner, J., Köhler, P. et al. (2014) Prospects for chlorophyll fluorescence remote sensing from the Orbiting Carbon Observatory-2. *Remote Sensing of Environment*, **147**, 1–12. <https://doi.org/10.1016/j.rse.2014.02.007>
- Galmés, J., Medrano, H. & Flexas, J. (2007) Photosynthetic limitations in response to water stress and recovery in Mediterranean plants with different growth forms. *New Phytologist*, **175**, 81–93. <https://doi.org/10.1111/j.1469-8137.2007.02087>
- Gatti, L.V., Gloor, M., Miller, J.B., Doughty, C.E., Malhi, Y., Domingues, L.G. et al. (2014) Drought sensitivity of Amazonian carbon balance revealed by atmospheric measurements. *Nature*, **506**, 76–80. <https://doi.org/10.1038/nature12957>
- Giardina, F., Konings, A.G., Kennedy, D., Alemohammad, S.H., Oliveira, R.S., Uriarte, M. et al. (2018) Tall Amazonian forests are less sensitive to precipitation variability. *Nature Geoscience*, **11**(6), 405. <https://doi.org/10.1038/s41561-018-0133-5>
- Guan, K., Pan, M., Li, H., Wolf, A., Wu, J., Medvigy, D. et al. (2015) Photosynthetic seasonality of global tropical forests constrained by hydroclimate. *Nature Geoscience*, **8**(4), 284. <https://doi.org/10.1038/ngeo2382>
- Hacke, U.G., Sperry, J.S., Pockman, W.T., Davis, S.D. & McCulloh, K.A. (2001) Trends in wood density and structure are linked to prevention of xylem implosion by negative pressure. *Oecologia*, **126**(4), 457–461. <https://doi.org/10.1007/s004420100628>
- Hansen, M.C., Potapov, P.V., Moore, R., Hancher, M., Turubanova, S.A., Tyukavina, A. et al. (2013) High-resolution global maps of 21st-century forest cover change. *Science*, **342**(6160), 850–853. <https://doi.org/10.1126/science.1244693>
- Hernández-Clemente, R., North, P.R., Hornero, A. & Zarco-Tejada, P.J. (2017) Assessing the effects of forest health on sun-induced chlorophyll fluorescence using the FluorFLIGHT 3-D radiative transfer model to account for forest structure. *Remote Sensing of Environment*, **193**, 165–179. <https://doi.org/10.1016/j.rse.2017.02.012>
- Huete, A.R., Didan, K., Shimabukuro, Y.E., Ratana, P., Saleska, S.R., Hutyra, L.R. et al. (2006) Amazon rainforests green-up with sunlight in dry season. *Geophysical Research Letters*, **33**(6), L06405. <https://doi.org/10.1029/2005GL025583>
- Humphrey, V. & Gudmundsson, L. (2019) GRACE-REC: a reconstruction of climate-driven water storage changes over the last century. *Earth System Science Data*, **11**(3), 1153–1170. <https://doi.org/10.5194/essd-11-1153-2019>
- Jackson, T.J. & Schmugge, T.J. (1991) Vegetation effects on the microwave emission of soils. *Remote Sensing of Environment*, **36**(3), 203–212. [https://doi.org/10.1016/0034-4257\(91\)90057-D](https://doi.org/10.1016/0034-4257(91)90057-D)
- Jimenezmunoz, J.C., Mattar, C., Barichivich, J., Santamariaartigas, A., Takahashi, K., Malhi, Y. et al. (2016) Record-breaking warming and extreme drought in the Amazon rainforest during the course of El Niño 2015–2016. *Scientific Reports*, **6**(1), 33130. <https://doi.org/10.1038/sre p33130>
- Joiner, J., Guanter, L., Lindstrot, R., Voigt, M., Vasilkov, A.P., Middleton, E.M. et al. (2013) Global monitoring of terrestrial chlorophyll fluorescence from moderate-spectral-resolution near-infrared satellite measurements: methodology, simulations, and application to GOME-2. *Atmospheric Measurement Techniques*, **6**(10), 2803–2823. <https://doi.org/10.5194/amt-6-2803-2013>
- Joiner, J., Yoshida, Y., Guanter, L. & Middleton, E.M. (2016) New methods for the retrieval of chlorophyll red fluorescence from hyperspectral satellite instruments: simulations and application to GOME-2 and SCIAMACHY. *Atmospheric Measurement Techniques*, **9**(8), 2016. <https://doi.org/10.5194/amt-9-3939-2016>
- Jones, M.O., Kimball, J.S. & Nemani, R.R. (2014) Asynchronous Amazon forest canopy phenology indicates adaptation to both water and light availability. *Environmental Research Letters*, **9**(12), 124021.
- Konings, A.G. & Gentine, P. (2017) Global variations in ecosystem-scale isohydricity. *Global Change Biology*, **23**(2), 891–905. <https://doi.org/10.1111/gcb.13389>

- Lee, J.E. & Boyce, K. (2010) Impact of the hydraulic capacity of plants on water and carbon fluxes in tropical South America. *Journal of Geophysical Research: Atmospheres*, **115** (D23), <https://doi.org/10.1029/2010JD014568>
- Lee, J.E., Frankenber, C., van der Tol, C., Berry, J.A., Guanter, L., Boyce, C.K. et al. (2013) Forest productivity and water stress in Amazonia: observations from GOSAT chlorophyll fluorescence. *Proceedings of the Royal Society B: Biological Sciences*, **280**(1761), 20130171. <https://doi.org/10.1098/rspb.2013.0171>
- Lewis, S.L., Brando, P.M., Phillips, O.L., van der Heijden, G.M. & Nepstad, D. (2011) The 2010 Amazon drought. *Science*, **331**(6017), 554. <https://doi.org/10.1126/science.1200807>
- Lima, C.H.R. & AghaKouchak, A. (2017) Droughts in Amazonia: spatiotemporal variability, teleconnections, and seasonal predictions. *Water Resources Research*, **53**, 10824–10840. <https://doi.org/10.1002/2016WR020086>
- Liu, H., Gleason, S.M., Hao, G., Hua, L., He, P., Goldstein, G. et al. (2019) Hydraulic traits are coordinated with maximum plant height at the global scale. *Science Advances*, **5**, eaav1332. <https://doi.org/10.1126/sciadv.aav1332>
- Liu, J., Bowman, K.W., Schimel, D.S., Parazoo, N.C., Jiang, Z., Lee, M. et al. (2017) Contrasting carbon cycle responses of the tropical continents to the 2015–2016 El Niño. *Science*, **358**, 191.
- Liu, L., Zhao, J. & Guan, L. (2013) Tracking photosynthetic injury of Paraquat-treated crop using chlorophyll fluorescence from hyperspectral data. *European Journal of Remote Sensing*, **46**, 459–473. <https://doi.org/10.5721/EuJRS20134627>
- Liu, Y.Y., Van Dijk, A.I., De Jeu, R., Canadell, J.G., Mccabe, M.F., Evans, J.P. et al. (2015) Recent reversal in loss of global terrestrial biomass. *Nature Climate Change*, **5**, 470–474. <https://doi.org/10.1038/nclimate2581>
- Liu, Y.Y., Van Dijk, A.I., Miralles, D.G., Mccabe, M.F., Evans, J.P., De Jeu, R.A.M. et al. (2018) Enhanced canopy growth precedes senescence in 2005 and 2010 Amazonian droughts. *Remote Sensing of Environment*, **211**, 26–37. <https://doi.org/10.1016/j.rse.2018.03.035>
- Lopes, A.P., Nelson, B.W., Wu, J., de Alencastro Graça, P.M.L., Tavares, J.V., Prohaska, N. et al. (2016) Leaf flush drives dry season green-up of the Central Amazon. *Remote Sensing of Environment*, **182**, 90–98. <https://doi.org/10.1016/j.rse.2016.05.009>
- Lott, F.C., Christidis, N. & Stott, P.A. (2013) Can the 2011 East African drought be attributed to human-induced climate change? *Geophysical Research Letters*, **40**(6), 1177–1181. <https://doi.org/10.1002/grl.50235>
- Malhi, Y., Aragão, L.E., Galbraith, D., Huntingford, C., Fisher, R., Zelazowski, P. et al. (2009) Exploring the likelihood and mechanism of a climate-change-induced dieback of the Amazon rainforest. *Proceedings of the National Academy of Sciences of the United States of America*, **106**, 20610–20615. <https://doi.org/10.1073/pnas.0804619106>
- Marengo, J.A., Nobre, C.A., Tomasella, J., Oyama, M.D., Sampaio de Oliveira, G., de Oliveira, R. et al. (2008) The drought of Amazonia in 2005. *Journal of Climate*, **21**(3), 495–516. <https://doi.org/10.1175/2007JCLI1600.1>
- Marengo, J.A., Tomasella, J., Alves, L.M., Soares, W.R. & Rodriguez, D.A. (2011) The drought of 2010 in the context of historical droughts in the Amazon region. *Geophysical Research Letters*, **38**(12), n/a–n/a. <https://doi.org/10.1029/2011GL047436>
- McDowell, N., Barnard, H., Bond, B., Hincley, T., Hubbard, R., Ishii, H. et al. (2002) The relationship between tree height and leaf area: sapwood area ratio. *Oecologia*, **132**(1), 12–20. <https://doi.org/10.1007/s00442-002-0904-x>
- McDowell, N., Pockman, W.T., Allen, C.D., Breshears, D.D., Cobb, N., Kolb, T. et al. (2008) Mechanisms of plant survival and mortality during drought: why do some plants survive while others succumb to drought? *New Phytologist*, **178**, 719–739. <https://doi.org/10.1111/j.1469-8137.2008.02436.x>
- McKee, T.B., Doesken, N.J. & Kleist, J. (1993) The relationship of drought frequency and duration to time scales. Eighth Conference on Applied Climatology 6.
- McVicar, T.R. & Bierwirth, P.N. (2001) Rapidly assessing the 1997 drought in Papua New Guinea using composite AVHRR imagery. *International Journal of Remote Sensing*, **22** (11), 2109–2128. <https://doi.org/10.1080/01431160120728>
- Moesinger, L., Dorigo, W., de Jeu, R., van der Schalie, R., Scanlon, T., Teubner, I. et al. (2020) The global long-term microwave Vegetation Optical Depth Climate Archive (VODCA). *Earth System Science Data*, **12**(1), 177–196. <https://doi.org/10.5194/essd-12-177-2020>
- Morton, D.C., Nagol, J., Carabajal, C.C., Rosette, J., Palace, M., Cook, B.D. et al. (2014) Amazon forests maintain consistent canopy structure and greenness during the dry season. *Nature*, **506**, 221–224. <https://doi.org/10.1038/nature13006>
- National Center for Atmospheric Research/University Corporation for Atmospheric Research. (2013) Standardized Precipitation Index (SPI) for Global Land Surface (1949–2012). Research Data Archive at the National Center for Atmospheric Research, Computational and Information Systems Laboratory. <https://doi.org/10.5065/D6086397>, <https://climatedataguide.ucar.edu/climate-data/standardized-precipitation-index-spi>. [Accessed 01 12 2020].
- Nepstad, D.C., de Carvalho, C.R., Davidson, E.A., Jipp, P.H., Lefebvre, P.A., Negreiros, G.H. et al. (1994) The role of deep roots in the hydrological and carbon cycles of Amazonian forests and pastures. *Nature*, **3**, 666–669. <https://doi.org/10.1038/372666a0>
- Nepstad, D., Lefebvre, P., Lopes da Silva, U., Tomasella, J., Schlesinger, P., Solórzano, L. et al. (2004) Amazon drought and its implications for forest flammability and tree growth: a basin-wide analysis. *Global Change Biology*, **10**(5), 704–717. <https://doi.org/10.1073/pnas.0611338104>

- Novick, K.A., Ficklin, D.L., Stoy, P.C., Williams, C.A., Bohrer, G., Oishi, A.C. et al. (2016) The increasing importance of atmospheric demand for ecosystem water and carbon fluxes. *Nature Climate Change*, **6**(11), 1023–1027. <https://doi.org/10.1038/nclimate3114>
- Palmer, W.C. (1965) *Meteorological drought, research paper No. 45*. Washington, DC: US Department of Commerce Weather Bureau.
- Panisset, J., Libonati, R., Gouveia, C.M., Machadosilva, F., Franca, D., Franca, J.R. et al. (2018) Contrasting patterns of the extreme drought episodes of 2005, 2010 and 2015 in the Amazon Basin. *International Journal of Climatology*, **38**(2), 1096–1104. <https://doi.org/10.1002/joc.5224>
- Pastorello, G., Trotta, C., Canfora, E., Chu, H., Christianson, D., Cheah, Y.W. et al. (2020) The FLUXNET2015 dataset and the ONEFlux processing pipeline for eddy covariance data. *Scientific Data*, **7**, 225. <https://doi.org/10.1038/s41597-020-0534-3>
- Phillips, O.L., Aragao, L.E., Lewis, S.L., Fisher, J.B., Lloyd, J., Lopez-Gonzalez, G. et al. (2009) Drought sensitivity of the Amazon rainforest. *Science*, **323**(5919), 1344–1347. <https://doi.org/10.1126/science.1164033>
- Phillips, O.L., Van der Heijden, G., Lewis, S.L., López-González, G., Aragão, L.E.O.C., Lloyd, J. et al. (2010) Drought–mortality relationships for tropical forests. *New Phytologist*, **187**(3), 631–646. <https://doi.org/10.1111/j.1469-8137.2010.03359.x>
- Raphael, M.W., Benedict, M.M. & James, M.R. (2017) Analysis of spatial and temporal drought variability in a tropical river basin using Palmer Drought Severity Index (PDSI). *International Journal of Water Resources and Environmental Engineering*, **9**, 178–190. <https://doi.org/10.5897/IJWREE2017.0723>
- Reichstein, M., Tenhunen, J.D., Rouspard, O., Ourcival, J.-M., Rambal, S., Miglietta, F. et al. (2002) Severe drought effects on ecosystem CO<sub>2</sub> and H<sub>2</sub>O fluxes at three Mediterranean evergreen sites: revision of current hypotheses? *Global Change Biology*, **8**, 999–1017. <https://doi.org/10.1046/j.1365-2486.2002.00530.x>
- Rowland, L., da Costa, A.C.L., Galbraith, D.R., Oliveira, R.S., Binks, O.J., Oliveira, A.A.R. et al. (2015) Death from drought in tropical forests is triggered by hydraulics not carbon starvation. *Nature*, **528**(7580), 119. <https://doi.org/10.1038/nature15539>
- Saatchi, S., Asefi-Najafabady, S., Malhi, Y., Aragão, L.E., Anderson, L.O., Myneni, R.B. et al. (2013) Persistent effects of a severe drought on Amazonian forest canopy. *Proceedings of the National Academy of Sciences of the United States of America*, **110**(2), 565–570. <https://doi.org/10.1073/pnas.1204651110>
- Sakai, S., Harrison, R.D., Momose, K., Kuraji, K., Nagamasu, H., Yasunari, T. et al. (2006) Irregular droughts trigger mass flowering in aseasonal tropical forests in Asia. *American Journal of Botany*, **93**(8), 1134–1139. <https://doi.org/10.3732/ajb.93.8.1134>
- Sakschewski, B., von Bloh, W., Boit, A., Poorter, L., Peña-Claros, M., Heinke, J. et al. (2016) Resilience of Amazon forests emerges from plant trait diversity. *Nature Climate Change*, **6**, 1032–1036. <https://doi.org/10.1038/nclimate3109>
- Saleska, S.R., Didan, K., Huete, A. & Rocha, H.R. (2007) Amazon forests green-up during 2005 drought. *Science*, **318**(5850), 612. <https://doi.org/10.1126/science.1146663>
- Saleska, S.R., Wu, J., Guan, K., Araujo, A.C., Huete, A., Nobre, A.D. et al. (2016) Dry-season greening of Amazon forests. *Nature*, **531**(7594), E4. <https://doi.org/10.1038/nature16457>
- Samanta, A., Ganguly, S. & Myneni, R.B. (2011) MODIS Enhanced Vegetation Index data do not show greening of Amazon forests during the 2005 drought. *New Phytologist*, **189**(1), 11–15. <https://doi.org/10.1111/j.1469-8137.2010.03516.x>
- Samanta, A., Ganguly, S., Hashimoto, H., Devadiga, S., Vermote, E., Knyazikhin, Y. et al. (2010) Amazon forests did not green-up during the 2005 drought. *Geophysical Research Letters*, **37**, n/a–n/a. <https://doi.org/10.1029/2009GL042154>
- Schimel, D., Pavlick, R., Fisher, J.B., Asner, G.P., Saatchi, S., Townsend, P. et al. (2015) Observing terrestrial ecosystems and the carbon cycle from space. *Global Change Biology*, **21**, 1762–1776. <https://doi.org/10.1111/gcb.12822>
- Shi, J., Jackson, T., Tao, J., Du, J., Bindlish, R., Lu, L. et al. (2008) Microwave vegetation indices for short vegetation covers from satellite passive microwave sensor AMSR-E. *Remote Sensing of Environment*, **112**, 4285–4300. <https://doi.org/10.1016/j.rse.2008.07.015>
- Sulla-Menashe, D. & Friedl, M.A. (2018) *User guide to collection 6 MODIS land cover (MCD12Q1 and MCD12C1) product*. Reston, VA, USA: USGS.
- Tian, F., Wigneron, J.-P., Ciais, P., Chave, J., Ogée, J., Peñuelas, J. et al. (2018) Coupling of ecosystem-scale plant water storage and leaf phenology observed by satellite. *Nature Ecology and Evolution*, **2**, 1428–1435. <https://doi.org/10.1038/s41559-018-0630-3>
- Van de Griend, A.A. & Wigneron, J.P. (2004) The b-factor as a function of frequency and canopy type at H-polarization. *IEEE Transactions on Geoscience and Remote Sensing*, **42**, 786–794. <https://doi.org/10.1109/TGRS.2003.821889>
- Van Emmerik, T., Steeledunne, S.C., Paget, A., Oliveira, R.S., Bittencourt, P.R., Barros, F.D. et al. (2017) Water stress detection in the Amazon using radar. *Geophysical Research Letters*, **44**(13), 6841–6849. <https://doi.org/10.1002/2017GL073747>
- Viovy, N. (2018) CRUNCEP Version 7 - Atmospheric Forcing Data for the Community Land Model. Research Data Archive at the National Center for Atmospheric Research, Computational and Information Systems Laboratory. <https://doi.org/10.5065/PZ8F-F017>

- Wang, X., Piao, S., Ciais, P., Friedlingstein, P., Myneni, R.B., Cox, P. et al. (2014) A two-fold increase of carbon cycle sensitivity to tropical temperature variations. *Nature*, **506** (7487), 212. <https://doi.org/10.1038/nature12915>
- Wigneron, J.P., Fan, L., Ciais, P., Bastos, A., Brandt, M., Chave, J. et al. (2020) Tropical forests did not recover from the strong 2015–2016 El Niño event. *Science Advances*, **6**(6), eaay4603. <https://doi.org/10.1126/sciadv.aay4603>
- Wolf, S., Keenan, T.F., Fisher, J.B., Baldocchi, D.D., Desai, A.R., Richardson, A.D. et al. (2016) Warm spring reduced carbon cycle impact of the 2012 US summer drought. *Proceedings of the National Academy of Sciences of the United States of America*, **113**(21), 5880–5885.
- Wu, J., Kobayashi, H., Stark, S.C., Meng, R., Guan, K., Tran, N.N. et al. (2018) Biological processes dominate seasonality of remotely sensed canopy greenness in an Amazon evergreen forest. *New Phytologist*, **217**(4), 1507–1520. <https://doi.org/10.1111/nph.14939>
- Xiao, X., Zhang, Q., Saleska, S., Hutyrá, L., De Camargo, P., Wofsy, S. et al. (2005) Satellite-based modeling of gross primary production in a seasonally moist tropical evergreen forest. *Remote Sensing of Environment*, **94**(1), 105–122. <https://doi.org/10.1016/j.rse.2004.08.015>
- Xu, L., Saatchi, S.S., Yang, Y., Myneni, R.B., Frankenberg, C., Chowdhury, D. et al. (2015) Satellite observation of tropical forest seasonality: spatial patterns of carbon exchange in Amazonia. *Environmental Research Letters*, **10**(8), 084005. <https://doi.org/10.1088/1748-9326/10/8/084005>
- Xu, L., Samanta, A., Costa, M.H., Ganguly, S., Nemani, R.R. & Myneni, R.B. (2011) Widespread decline in greenness of Amazonian vegetation due to the 2010 drought. *Geophysical Research Letters*, **38**, n/a–n/a. <https://doi.org/10.1029/2011GL046824>
- Yang, J., Tian, H., Pan, S., Chen, G., Zhang, B. & Dangal, S. (2018a) Amazon drought and forest response: largely reduced forest photosynthesis but slightly increased canopy greenness during the extreme drought of 2015/2016. *Global Change Biology*, **24**, 1919–1934. <https://doi.org/10.1111/gcb.14056>
- Yang, Y., Saatchi, S.S., Xu, L., Yu, Y., Choi, S., Phillips, N. et al. (2018b) Post-drought decline of the Amazon carbon sink. *Nature Communications*, **9**(1), 3172. <https://doi.org/10.1038/s41467-018-05668-6>
- Yoo, S.H., Ho, C.H., Yang, S., Choi, H.J. & Jhun, J.G. (2004) Influences of tropical western and extratropical Pacific SST on East and Southeast Asian climate in the summers of 1993–94. *Journal of Climate*, **17**(13), 2673–2687. [https://doi.org/10.1175/1520-0442\(2004\)017<2673:IOTWAE>2.0.CO;2](https://doi.org/10.1175/1520-0442(2004)017<2673:IOTWAE>2.0.CO;2)
- Yuan, W., Zheng, Y., Piao, S., Ciais, P., Lombardozzi, D., Wang, Y. et al. (2019) Increased atmospheric vapor pressure deficit reduces global vegetation growth. *Science Advances*, **5**, eaax1396. <https://doi.org/10.1126/sciadv.aax1396>
- Zhang, Y., Joiner, J., Alemohammad, S.H., Zhou, S. & Gentine, P. (2018a) A global spatially contiguous solar-induced fluorescence (CSIF) dataset using neural networks. *Biogeosciences*, **15**(19), 5779–5800. <https://doi.org/10.5194/bg-15-5779-2018>
- Zhang, Y., Joiner, J., Gentine, P. & Zhou, S. (2018b) Reduced solar-induced chlorophyll fluorescence from GOME-2 during Amazon drought caused by dataset artifacts. *Global Change Biology*, **24**(6), 2229–2230. <https://doi.org/10.1111/gcb.14134>
- Zhang, Y., Zhu, Z., Liu, Z., Zeng, Z., Ciais, P., Huang, M. et al. (2016) Seasonal and interannual changes in vegetation activity of tropical forests in Southeast Asia. *Agricultural and Forest Meteorology*, **224**, 1–10. <https://doi.org/10.1016/j.agrformet.2016.04.009>
- Zhao, M. & Running, S.W. (2010) Drought-induced reduction in global terrestrial net primary production from 2000 through 2009. *Science*, **329**(5994), 940–943. <https://doi.org/10.1126/science.1192666>
- Zhou, L., Tian, Y., Myneni, R.B., Ciais, P., Saatchi, S., Liu, Y.Y. et al. (2014) Widespread decline of Congo rainforest greenness in the past decade. *Nature*, **509**, 86–90. <https://doi.org/10.1038/nature13265>
- Zhu, Z., Bi, J., Pan, Y., Ganguly, S., Anav, A., Xu, L. et al. (2013) Global data sets of vegetation leaf area index (LAI)3g and fraction of photosynthetically active radiation (FPAR)3g derived from global inventory modeling and mapping studies (GIMMS) normalized difference vegetation index (NDVI3g) for the period 1981 to 2011. *Remote Sensing*, **5**, 927–948. <https://doi.org/10.3390/rs5020927>

## Supporting Information

Additional supporting information may be found online in the Supporting Information section at the end of the article.

**Figure S1.** Drought loss ( $\Delta\text{CGP}_{\text{drought}}$ ) of forest canopy growth proxies (CGPs) during the drought period (A–D) and post-drought gain ( $\Delta\text{CGP}_{\text{recovery}}$ ) after droughts (E–J) against the corresponding CGPs of the recovery years.

**Figure S2.** Scatter diagrams between  $\Delta\text{GIMMS}$  LAI and corresponding climatic interannual dynamics (i.e.,  $\Delta\text{Tair}$ ,  $\Delta\text{SWdown}$ ,  $\Delta\text{VPD}$ ,  $\Delta\text{PRE}$ , and  $\Delta\text{TWS}$ ).

**Figure S3.** Scatter diagrams between  $\Delta\text{MODIS}$  NIRv and corresponding climatic interannual dynamics (i.e.,  $\Delta\text{Tair}$ ,  $\Delta\text{SWdown}$ ,  $\Delta\text{VPD}$ ,  $\Delta\text{PRE}$ , and  $\Delta\text{TWS}$ ).

**Figure S4.** Scatter diagrams between  $\Delta\text{CSIF}$  and corresponding climatic interannual dynamics (i.e.,  $\Delta\text{Tair}$ ,  $\Delta\text{SWdown}$ ,  $\Delta\text{VPD}$ ,  $\Delta\text{PRE}$ , and  $\Delta\text{TWS}$ ).

**Figure S5.** Scatter diagrams between  $\Delta\text{Ku-VOD}$  and corresponding climatic interannual dynamics (i.e.,  $\Delta\text{Tair}$ ,  $\Delta\text{SWdown}$ ,  $\Delta\text{VPD}$ ,  $\Delta\text{PRE}$ , and  $\Delta\text{TWS}$ ).

**Figure S6.** In situ observed sensitivity of GPP and LE to (A and D) SWdown, (B and E) VPD, and (C and F) PRE as functions of  $\text{GPP}_{\text{recovery}}$  and  $\text{LE}_{\text{recovery}}$ .

**Figure S7.** Long-term interannual dynamics of  $\text{Drought}_{\text{fraction}}$  calculated from PDSI (black solid lines), SPI with 3 months time scale (SPI3, orange dash lines), SPI with 6 months time scale (SPI6, green dash lines), and SPI with 12 months time scale (SPI12, purple dash lines) from 1985 to 2012.

**Figure S8.** The correlation between  $\text{Drought}_{\text{fraction}}$  from PDSI and  $\text{Drought}_{\text{fraction}}$  from SPI3 (orange), SPI6 (green), SPI12 (purple).

**Figure S9.** Spatial pattern of PDSI anomaly during 2005 JAS Amazon southwest drought.

Figure S10. Monthly  $\text{Drought}_{\text{fraction}}$  of Amazon in 2003 (red solid line) and 2005 (black solid line).

**Table S1.** Information of all of the data used in this study.

**Table S2.** Basic information of 3 in-situ sites from Fluxnet2015.

**Table S3.** Historical drought years across tropical Amazon, Africa, and Asia.

**Table S4.** Correlation analysis between CGP ( $\Delta\text{CGP}$ ) and PDSI ( $\Delta\text{PDSI}$ ) interannual dynamics.

**Table S5.** Statistics of percentage of High-CGP and Low-CGP of each continent (Fig. 7).

**Table S6.** Correlations between interannual dynamics in canopy growth ( $\Delta\text{CGPs}$ ) of High-CGPs trees and climatic interannual variations ( $\Delta\text{Tair}$ ,  $\Delta\text{SWdown}$ ,  $\Delta\text{VPD}$ ,  $\Delta\text{PRE}$ , and  $\Delta\text{TWS}$ ).

**Table S7.** Correlations between interannual dynamics in canopy growth ( $\Delta\text{CGPs}$ ) of Low-CGPs trees and climatic interannual variations ( $\Delta\text{Tair}$ ,  $\Delta\text{SWdown}$ ,  $\Delta\text{VPD}$ ,  $\Delta\text{PRE}$ , and  $\Delta\text{TWS}$ ).

**Table S8.** The statistics of in-situ observed sensitivity (represented by the slope of linear regression) of  $\text{GPP}/\text{LE}$  ( $\text{GPP}_{\text{recovery}}/\text{LE}_{\text{recovery}}$ ) to  $\text{SWdown}$  ( $\frac{\Delta\text{GPP}}{\Delta\text{SWdown}}$ ,  $\frac{\Delta\text{LE}}{\Delta\text{SWdown}}$ ),  $\text{VPD}$  ( $\frac{\Delta\text{GPP}}{\Delta\text{VPD}}$ ,  $\frac{\Delta\text{LE}}{\Delta\text{VPD}}$ ), and  $\text{PRE}$  ( $\frac{\Delta\text{GPP}}{\Delta\text{PRE}}$ ,  $\frac{\Delta\text{LE}}{\Delta\text{PRE}}$ ).